We are IntechOpen, the world's leading publisher of Open Access books Built by scientists, for scientists

6,900
Open access books available

186,000
International authors and editors

200M
Downloads

154
Countries delivered to

Our authors are among the

TOP 1%
most cited scientists

12.2%
Contributors from top 500 universities

CLARIVATE ANALYTICS
BOOK CITATION INDEX
INDEXED

WEB OF SCIENCE™

Selection of our books indexed in the Book Citation Index
in Web of Science™ Core Collection (BKCI)

Interested in publishing with us?
Contact book.department@intechopen.com

Numbers displayed above are based on latest data collected.
For more information visit www.intechopen.com

Aluminium Nitride thin Film Acoustic Wave Device for Microfluidic and Biosensing Applications

Y.Q. Fu[1], J. S. Cherng[2], J. K. Luo[3], M.P.Y. Desmulliez[1], Y. Li[4],
A. J. Walton[4] and F. Placido[5]

[1]*School of Engineering and Physical Sciences, Institute of Integrated Systems,*
Heriot-Watt University, Edinburgh, EH14 4AS,
[2]*Department of Materials Engineering,*
Mingchi University of Technology, Taishan, Taipei,
[3]*Centre for Material Research and Innovation, University of Bolton,*
Deane Road, Bolton, BL3 5AB,
[4]*Scottish Microelectronics Centre, School of Engineering, Institute of Integrated Systems,*
University of Edinburgh, Edinburgh, EH10 7AT,
[5]*Thin Film Centre, University of the West of Scotland, Paisley, PA1 2BE,*
[1,3,4,5]*UK*
[2]*Taiwan*

1. Introduction

When an alternating electric field is applied to an interdigitated transducer (IDT) on a piezoelectric material, an acoustic wave is generated. The wave can propagate in a direction perpendicular to the surface of the material into the bulk (bulk acoustic wave, BAW) or along the surface of the material (surface acoustic wave, SAW). This piezoelectric effect is manifested in either a Rayleigh mode (vertical and surface normal) or as a shear horizontal wave (in-plane) [Galipeau et al 1997]. The most commonly used bulk acoustic wave device is the Quartz Crystal Microbalance (QCM), which is generally made of quartz sandwiched between two electrodes. In contrast a surface acoustic wave propagating within a thin surface layer, which has a lower acoustic velocity than that of the piezoelectric substrate, is called a Love wave and such devices are typically operated in the Shear Horizontal (SH) wave mode. Waves propagating in a thin plate with a thickness much less than the acoustic wavelength are called a flexural plate or Lamb waves [Luginbuhl et al 1997]. These acoustic wave technologies and devices have been commercially exploited for more than 60 years in industrial applications [Ballantine et al 1996. Hoummady et al., 1997] and currently the telecommunications industry is one of the largest consumers, primarily in mobile phones and base stations, which account for ~3 billion acoustic wave filters annually. Other promising and growing applications include automotive applications (pressure acceleration, or shock sensors), medical applications (chemical sensors), and other industrial applications (including temperature, mass, viscosity, vapour and humidity sensors).

Most acoustic wave devices can be used as sensors because they are sensitive to mechanical, chemical, or electrical perturbations on the surface of the device [Lucklum & P. Hauptmann 2003, Grate et al 2003]. Acoustic wave sensors have the advantage that they are versatile, sensitive and reliable, being able to detect not only mass/density changes, but also viscosity, wave functions, elastic modulus, conductivity and dielectric properties. They have many applications in monitoring a large number of parameters which include pressure, moisture, temperature, force, acceleration, shock, viscosity, flow, pH, ionic contaminants, odour, radiation and electric fields [Shiokawa & Kondoh 2004, Wohltjen et al. 1997]. Recently, there has been an increasing interest in acoustic wave based biosensors to detect traces of biomolecules through specific bioreactions with biomarkers. These include DNA, proteins (enzymes, antibodies, and receptors), cells (microorganisms, animal and plant cells, cancer cells etc.), tissues, viruses, as well as the detection of chemical substances through specific chemical absorption layers [Cote et al 2003, Kuznestsova, and Coakley 2007, Teles & Fonseca 2003]. By detecting traces of associated molecules, it is possible to diagnose diseases and genetic disorders, prevent potential bioattachment, and monitor the spread of viruses and pandemics [Vellekoop 1998, Shiokawa & Kondoh 2004, Gizeli 1997]. Compared with other common bio-sensing technologies, such as surface plasmon resonance (SPR), optical fibres, and sensors based on field effect transistors or cantilever-based detectors, acoustic wave based technologies have the combined advantages of simple operation, high sensitivity, small size and low cost, with no need for bulky optical detection systems [Lange et al 2008].

By far the most commonly reported acoustic wave based biosensor is QCM [Markx, 2003], which can be operated in a liquid environment using a thickness shear-mode. The advantages of QCM include: (1) simplicity in design and (2) a high Q factor. However, less attractive features of QCM biosensors are a low detection resolution due to the low operating frequency in the range of 5~20 MHz and a large base mass; a thick substrate (0.5~1 mm) and large surface area (>1 cm²) which cannot easily be scaled down. In contract SAW based biosensors have their acoustic energy confined within a region about one wave length from the surface, and so the basemass of the active layer is roughly one order of magnitude smaller than that of the QCM. Therefore, the sensitivity of the SAW devices is dramatically larger than that of the QCM. The longitudinal or Rayleigh mode SAW device has a substantial surface-normal displacement that rapidly dissipates the acoustic wave energy into the liquid, leading to excessive damping, and hence poor sensitivity and noise. However, waves in a SH-SAW device propagate in a shear horizontal mode, and therefore do not easily radiate acoustic energy into the liquid [Barie & Rapp 2001, Kovacs & Venema 1992] and hence the device maintains a high sensitivity in liquids. Consequently SH-SAW devices are particularly well suitable for bio-detection, especially for "real-time" monitoring. In most cases, Love wave devices operate in the SH wave mode with the acoustic energy trapped within a thin waveguide layer (typically sub-micron). This enhances the detection sensitivity by more than two orders of magnitude compared with a conventional SAW device owing to their much reduced base mass [Josse et al 2001, Mchale 2003]. They are therefore frequently employed to perform biosensing in liquid conditions [Lindner 2008, Kovacs et al 1992, Jacoby & Vellekoop 1997].

Acoustic wave technologies are also particularly well suited to mixing and pumping and as a result are an attractive option for microfluidics applications [Luo et al 2009]. Taking the SAW device as one example, Rayleigh-based SAW waves have a longitudinal component that can be coupled with a medium in contact with the surface of the device. When liquid

(either in bulk or droplet form) exists on the surface of a SAW device, the energy and momentum of the acoustic wave are coupled into the fluid with a Rayleigh angle, following Snell's law of refraction (see Fig. 1) [Wixforth 2004, Shiokawa et al 1989]. The Rayleigh angle, θ, is defined by

$$\theta = \sin^{-1}\left(\frac{v_l}{v_S}\right) \qquad (2)$$

where v_l and v_s are the velocities of the longitudinal wave in solid and liquid. The generated acoustic pressure can create significant acoustic streaming in a liquid which can be used to enable liquid mixing, pumping, ejection and atomization [Newton et al 1999]. This pressure facilitates rapid liquid movement and also internal agitation, which can be used to speed up biochemical reactions, minimize non-specific bio-binding, and accelerate hybridization reactions in protein and DNA analysis which are routinely used in proteomics and genomics [Toegl et al 2003, Wixforth et al 2004]. Surface acoustic wave based liquid pumps and mixers [Tseng et al 2006, Sritharan et al 2006], droplet positioning and manipulation [Sano et al 1998], droplet ejection and atomization systems [Chono et al 2004, Murochi et al 2007], and fluidic dispenser arrays [Strobl et al 2004] have been proposed and developed. They have distinct advantages, such as a simple device structure, no moving-parts, electronic control, high speed, programmability, manufacturability, remote control, compactness and high frequency response [Renaudin et al 2006, Togle et al 2004, Franke & Wixforth 2008].
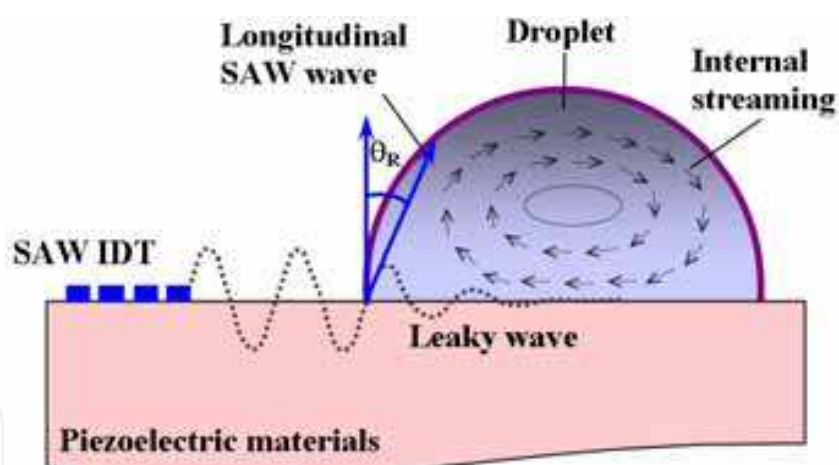

Fig. 1. Principle of surface acoustic wave streaming effect: interaction between propagating surface acoustic wave and a liquid droplet causing acoustic streaming inside droplet

Acoustic wave devices can be used for both biosensing and microfluidics applications, which are two of the major components for lab-on-a-chip systems. Therefore, it is attractive to develop lab-on-chip bio-detection platforms using acoustic wave devices as this integrates the functions of microdroplet transportation, mixing and bio-detection. To date, most of the acoustic devices have been made from bulk piezoelectric materials, such as quartz (SiO_2), lithium tantalate ($LiTaO_3$), lithium niobate ($LiNbO_3$) and sapphire (Al_2O_3). These bulk materials are expensive, and are less easily integrated with electronics for control and signal processing. Piezoelectric thin films such as PZT, ZnO and AlN have good

piezoelectric properties, high electro-mechanical coupling coefficient, high sensitivity and reliability [Pearton et al 2005]. They can be grown in thin film form on a variety of substrates, which include silicon, making these materials promising for integration with electronic circuitry, particularly for devices aimed for one-time use, low-price and mass production [Muralt 2008] (see Table 1). Amongst these, PZT has the highest piezoelectric constant and electromechanical coupling coefficient. However, for biosensing applications, PZT films have disadvantages such as higher acoustic wave attenuation, lower sound wave velocities, poor biocompatibility and worst of all, the requirement for extremely high temperature sintering and high electric field polarization, which make them largely unsuitable for integration with electronics (see Table 1). ZnO shows a high piezoelectric coupling, and it is easy to control the film stoichiometry, texture and other properties compared with that for AlN film [Jagadish & Pearton 2006]. Zinc oxide is considered

Materials	ZnO	AlN	PZT	Quartz	128° cut LiNbO$_3$	36° cut LiTaO$_3$	PVDF
Density (g/cm³)	5.61	3.3	7.8	2.64	4.64	7.45	1.79
Moulus (GPa)	110-140	300-350	61	71.7		225	0.16
Hardness	4-5 GPa	15 GPa	7-18 GPa	Moh's 7	Moh's 5 Knoop 800-1000	70-110 Knoop 700-1200	Shore D75-85
refractive index	1.9 to 2.0	1.96	2.40	1.46	2.29	2.18	1.42
Piezo-constant d33 (pC/N)	12	4.5, 6.4	289-380, 117	2.3(d11)	19-27	-21	-35
Coupling coefficient, k	0.15-0.33	0.17-0.5	0.49	0.0014	0.23	0.2	0.12-0.2
Effective coupling coefficient, k² (%)	1.5-1.7	3.1-8	20-35	8.8-16	2-11.3	0.66-0.77	2.9
Acoustic velocity by transverse (m/s)	6336 (2650)	11050 (6090)	4500 (2200)	5960 (3310)	3970	3230-3295	2600
Dielectric constant	8.66	8.5-10	380	4.3	85 (29)	54 (43)	6-8
Coefficient of thermal expansion (CTE, x10⁻⁶)	4	5.2	1.75	5.5	15	-16.5	42-75

Table 1. Comparison of common piezoelectric materials [Fu et al 2010]

biosafe and therefore suitable for biomedical applications that immobilize and modify biomolecules [Kumar & Shen 2008]. A summary of the recent development on ZnO film based microfluidics and sensing have been reported by Fu et al 2010. Currently, there is some concern that ZnO film is reactive, and unstable even in air or moisture and the stability and reliability is potentially a major problem.

AlN has a very large volume resistivity and is a hard material with a bulk hardness similar to quartz, and is also chemically stable to attack by atmospheric gases at temperatures less than 700ºC. Compared with ZnO, AlN also shows a slightly lower piezoelectric coupling. However, the Rayleigh wave phase velocity in AlN is much higher than that in ZnO, which suggests that AlN is better for high frequency and high sensitivity applications [Lee et al 2004]. The combination of its physical and chemical properties is consequently promising for practical applications of AlN both in bulk and thin-film forms. Using AlN potentially enables the development of acoustic devices operating at higher frequencies, with improved sensitivity and performance (insertion loss and resistance) in harsh environments [Wingqvist et al 2007a]. AlN thin films have other attractive properties such as high thermal conductivity, good electrical isolation and a wide band gap (6.2 eV). Therefore, AlN thin films have been used, not only for the surface passivation of semiconductors and insulators, but also for both optical devices in the ultraviolet spectral region and acousto-optic devices.

This chapter will focus on reviewing recent progress covering the issues related to AlN film preparation, its microstructure, piezoelectric properties and device fabrication as well as applications related to microfluidcis and biosensing.

2. AlN film processing and characterization

The AlN crystal belongs to a hexagonal class or a distorted tetrahedron (see Fig. 2), with each Al atom surrounded by four N atoms [Chiu et al 2007]. The four Al–N bonds can be categorized into two types: three are equivalent Al–N$_{(x)}$ (x = 1, 2, 3) bonds, B$_1$, and one is a unique Al–N bond, B$_2$, in the c-axis direction or the (002) orientation. Since the B$_2$ is more ionic, it has a lower bonding energy than the other bonds [Chiu et al 2007]. The highest value of $K_t{}^2$ and the piezoelectric constant are in the c-axis direction, thus the AlN film growing with c-axis orientation has much better piezoelectricity when an acoustic wave device is excited in the film thickness direction.

2.1 AlN deposition methods

Many different methods have been used to prepare AlN films. These include chemical vapour deposition (CVD) or plasma enhanced CVD (PECVD) [Sanchez et al 2008, Tanosch et al 2006, Ishihara et al 2000, Liu et al 2003], filtered arc vacuum arc (FAVC) [Ji et al 2004], molecular beam deposition (MBE) [Kern et al 1998], hydride vapour phase epitaxy (HVPE) [Kumagai et al 2005], pulsed laser deposition (PLD) [Lu et al, 2000, Liu et al 2003, Baek et al 2007], and sputtering [Mortet et al 2003 and 2004, Auger et al 2005, Clement et al 2003]. Of these technologies, MBE can grow a single-crystal epitaxial AlN film with other advantages which include precise control over the deposition parameters, atomic scale control of film thickness and *in situ* diagnostic capabilities. However, it has limitations of low growth rate, expensive instrument setup and a high process temperature from 800 to 1000ºC. Unfortunately this results in thermal damage of the AlN layers during deposition, as well as the substrate depending on the material. CVD technology including metal organic CVD

(MOCVD) and PECVD is also of great interest for AlN film growth because it not only gives rise to high-quality films but also is applicable to large-scale production. However, its high process temperature (about 500 to 1000 °C) may be inappropriate for CMOS-compatible processes and this causes large thermal stresses in the films, which potentially restricts the choice of substrate. The main advantages of PLD are its ability to create high-energy source particles, permitting high-quality film growth at potentially low substrate temperatures (typically ranging from 200 to 800 °C) in high ambient gas pressures in the 10^{-5}–10^{-1} Torr range. One disadvantages of PLD is its limited deposition size and uniformity.
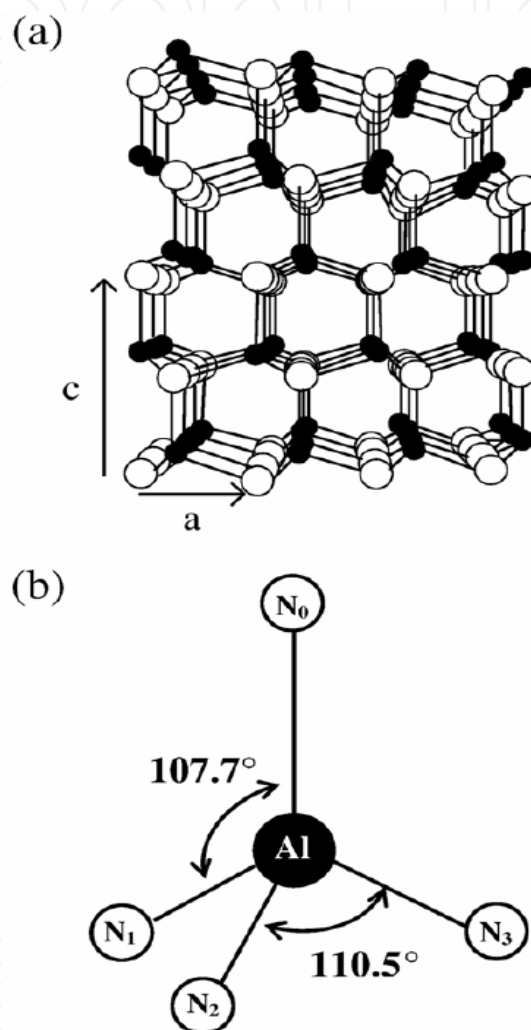
Fig. 2. (a) Hexagonal structure of AlN and (b) tetrahedral structure, with one Al atom surrounded by four N atoms [Chiu et al 2007].

One of the most popular thin film deposition techniques for AlN films is sputtering (DC, radio-frequency magnetron and reactive sputtering). They can be deposited in an N_2/Ar reactive atmosphere by DC reactive sputtering pure Al, or by RF sputtering using an AlN target. Sputtering methods can deposit a good crystalline AlN thin film at a relatively low temperature (between 25 °C and 500 °C) and the sputtered films normally exhibit good epitaxial film structure [Engelmark et al 2000]. DC Sputtering using an Al target can result in "target poisoning" caused by the accumulation of charging on the target, which causes arcing or a decrease in the sputtering rate. Switching the choice of power supply from DC to

RF addresses this problem, but at the cost of lower deposition rate and more expensive and complex equipment. Pulsed-DC reactive sputtering provides a solution to this limitation and also brings other advantages, which include higher film uniformity and higher plasma activity [Cherng et al. 2007, 2008].

From a MEMS fabrication point of view, reactive sputtering is one of the best methods, with good reproducibility and compatibility with planar device fabrication technology. In this section, we will focus on the processing, texture and acoustic wave properties of the sputtered AlN films.

2.2 Influence of process parameters

The quality of the sputtered AlN thin films depends on plasma power, working pressure, substrate temperature, RF power and substrate materials. Increasing the RF power causes higher kinetic energy of adatoms when they arrive on the substrate, which provides enough energy for the formation of the (0 0 0 2) preferred orientation of AlN layers. On the other hand, increased RF power also raises the number of ejected species from the target, which results in an increased growth rate as a function of RF power.

Gas pressure potentially also has a significant influence on AlN film deposition with increasing the sputtering pressure up to 1.33 Pa being reported to improve the crystalline quality of the (0 0 0 2)-oriented AlN layers. However, it was also noted that further increases in the sputtering pressure degraded the crystalline quality [Gao et al 2007]. Increasing in the sputtering pressure will raise the probability of collisions between sputtered particles and nitrogen atoms simply because of more gas atoms are available for ionization. Therefore, the average energy of the sputtered particles is increased which improves the crystalline quality. However, further increase in sputtering pressure results in the reduction of mean free path of N or Ar ions, which leads to a reduction of the energy of sputtered and deposited atoms, thus degrading the crystalline quality [Gao et al 2007].

Okamoto et al 2000 observed a change of the preferred crystallographic orientation by increasing the N_2 partial pressure, and Baek et al. 2007 detected the same effect when the substrate temperature and N_2 gas fluence were changed. Sudhir et al. 1998 demonstrated that the surface morphology and structure of the AlN films can be actively controlled by adjusting the nitrogen partial pressure during the film deposition. They attributed the observed dependence of the structural quality to the change in the surface diffusion of adatoms, given by $L \sim (D\tau)^{1/2}$, where D is the diffusion coefficient and τ is the residence time of adatoms. Larger values of diffusion length imply more time for the adatoms to find energetically favourable lattice positions, thus reducing the density of surface defects and improving the crystal quality [Sudhir et al 1998].

Leong and Ong 2004 prepared reactive magnetron sputtered AlN films by varying parameters such as substrate temperature Ts, radio frequency power Pw, and substrate materials (including silicon, platinum coated silicon and sapphire). The effects of these parameters on film microstructure as a function of deposition temperature are shown in Fig. 3. This identifies the regions of nearly amorphous (na-) AlN, polycrystalline (p-) AlN, texture (t-) AlN and epitaxial (e-) AlN on three substrate materials, i.e. Si(100), Pt(111)/Si(100) and Al₂O₃(001), respectively. The 'na-AlN" means that the microstructure of AlN has a highly disordered matrix containing small randomly orientated crystals, which normally forms at a lower rf power, and low temperature [Leong & Ong 2004]. At higher temperature and power, the thermal energy gained by the depositing species is larger, and the atoms are more mobile. Hence, the species more readily aggregate and crystallize,

resulting in the formation of larger grains compared with those present in the na-AlN structure. Increases in Ts and Pw have the effects of increasing the thermal energy of the species on the substrate surface, and enhancing the crystallization of the deposits and preferential orientation of grains. It should be noted that sapphire substrate have better lattice matching with the AlN, which facilitates the epitaxial growth of the AlN structure [Leong & Ong 2004].
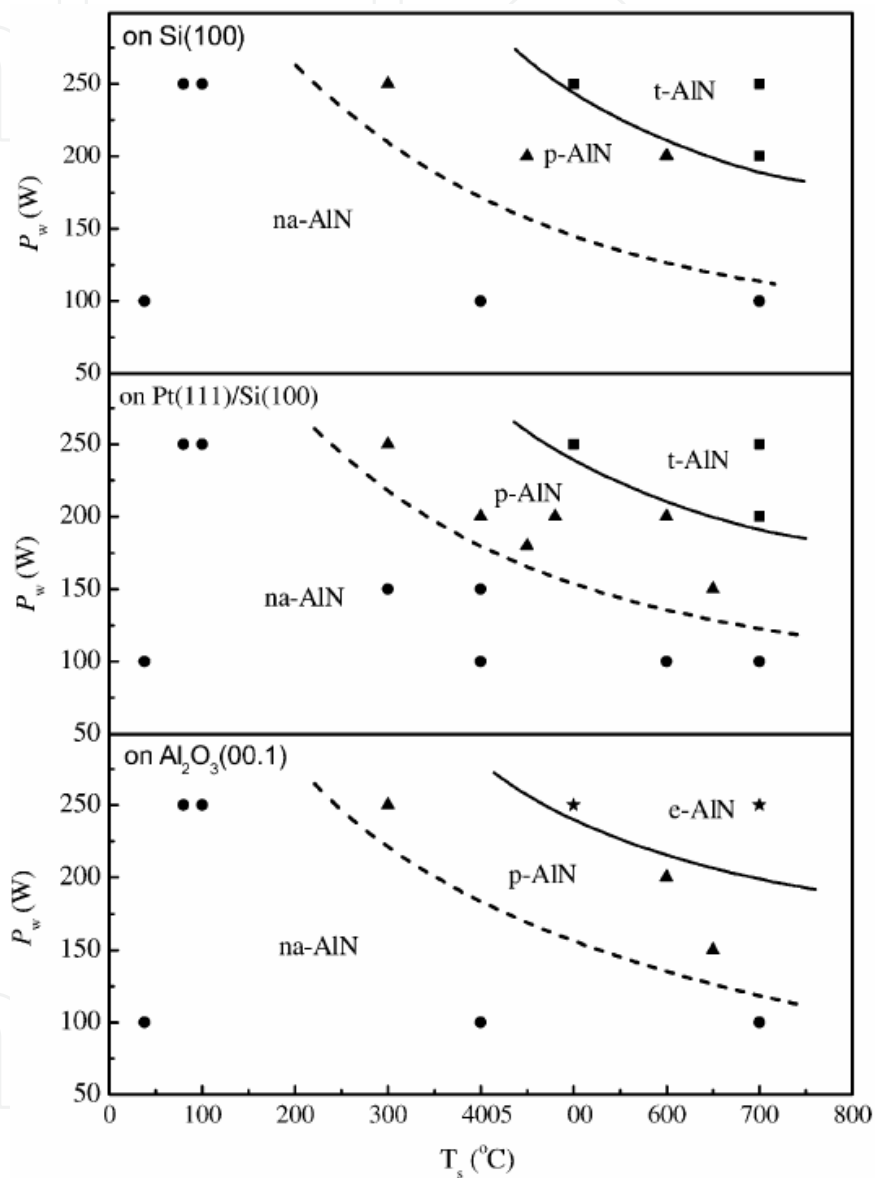

Fig. 3. Effects of the process parameters on film microstructure on three substrate materials, i.e. Si(100), Pt(111)/Si(100) and Al_2O_3(001) [Leung & Ong 2004]

Because of the reactivity of Al, a high-purity source Al material and an oxygen-free environment are required to grow high-quality AlN film [Vashaei et al 2009]. Hence, oxygen has a significant influence on AlN film growth during sputtering, and contamination due to residual oxygen or water can seriously interfere with the formation of the AlN film structure. Growth rate of the AlN film decrease with increased oxygen in the sputtering gas and their predominant polarity also changes from Al polarity to N polarity with increase in

the oxygen concentration [Vergara et al 2004, Cherng et al 2008 a and b]. Increased oxygen concentration in sputtering gas increases Al-O bonding, as the bonding energy of Al-O (511 kJ/mol) is higher than that of Al-N (230 kCal/mol) [Akiyama et al 2008], and formation of Al-O bond significantly deteriorates the piezoelectric response of the AlN films.

The quality of AlN films is affected by any contamination during sputtering [Cheung & Ong 2004], resulting from target impurity, gas impurity, and residual oxygen/moisture from both inside (adsorption) and outside (leakage) the working chamber. Out-gassing is a critical parameter that must be controlled for quality of AlN crystals, and effect of the out-gassing rate has been evaluated by observing the pressure increase with time after the designated base pressure has been reached and the pump was shut down (as shown in Fig. 4). The FWHM (full width of half maximum) from an X-ray diffraction rocking curve and the residual stress of the films has been obtained in order to compare the film quality [Cherng 2008 and 2009].
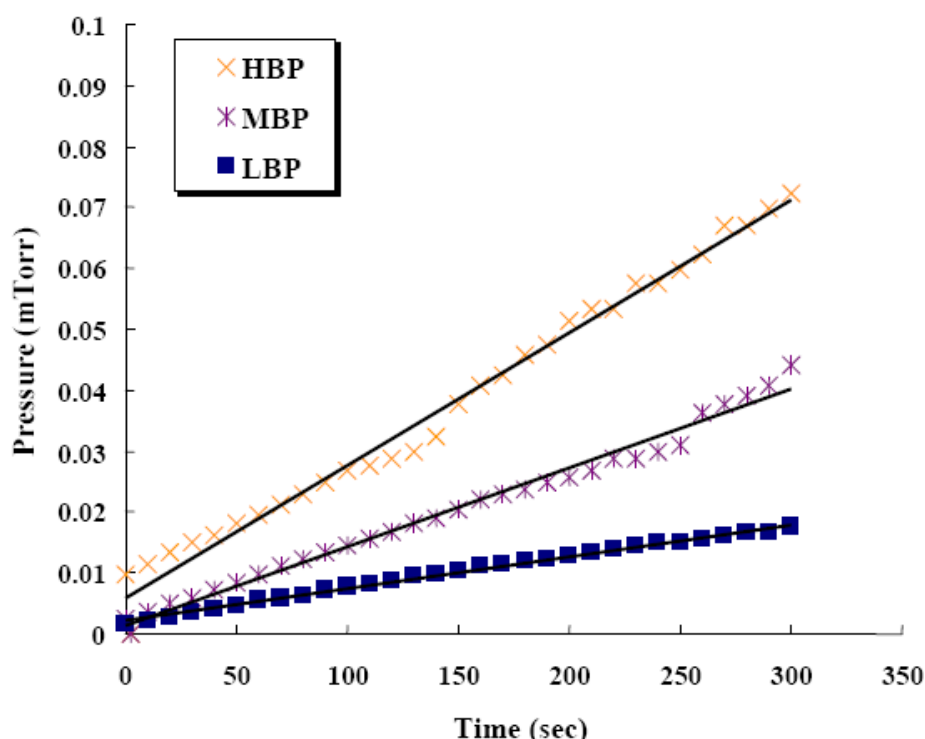

Fig. 4. Outgassing rate evaluated by observing the pressure increase with time after the designated base pressure was reached and the pump was shut down where the slope of each curve indicates its outgassing rate respectively. The sputtering system was either pumped down to a base pressure of 3×10^{-6} Torr (thus termed HBP, high base pressure) or 1×10^{-6} Torr (thus termed MBP, medium base pressure) or 4×10^{-7} Torr (thus termed LBP, low base pressure) before admitting the gas mixture in, in order to examine the effects of outgassing [Cherng & Chang, 2008]

Figures 5(a) and (b) show the effect of working pressure on FWMH and film stress at different outgasing levels. The FWHM decreases and residual stress becomes more compressive with decreasing working pressure. As the pressure is decreased, the mean free path of the sputtered atoms becomes comparable with the target-to-substrate distance (λ_{mfp}=5 / P, where λ_{mfp} is in cm and P in mTorr) [O'Hanlon 1989], and hence less gas phase scattering is observed. The result is that sputtered Al atoms arrive on the surface of the

growing film with most of their energy retained. They transfer a substantial amount of energy to the growing film, and thus increase the mobility of the adatoms and can then move to the lattice sites which form a closest-packed (0002) plane with the lowest surface energy. In fact, the energy delivered to the growing film is sufficiently high so that fully (0002)-textured (texture coefficient=1) AlN films with FWHM of the rocking curve lower than 2° are readily obtainable without substrate heating. In addition to the aforementioned "atom-assisted deposition" [Iriarte et al 2002], a second mechanism, namely, "atomic peening" [Windischmann 1992] is also at work. Since N atoms are lighter than Al, the reflection coefficient of N ions is high sufficient for a large fraction of them bombarding the Al target to be neutralized and reflected off the target surface upon impact. This results in additional bombardment of the growing film by energetic N neutrals. On the other hand, Ar ions are effectively not reflected since they are heavier than Al. Both the atom assisted deposition and atomic peening mechanisms require a sufficiently low working pressure so the energetic particles do not lose much of their energy while travelling through the gas phase. This explains why as the working pressure decreases, the FWHM of the rocking curve decreases and the residual stress becomes more compressive [Cherng & Chang, 2008]. Lower outgassing levels show a better figure-of-merit that not only the FWHM of the rocking curve is lower, but also the change of residual stress with pressure occurs in a much smoother manner and with much smaller magnitude. X-ray Photoelectron Spectroscopy (XPS) analyses for four selected samples circled in Fig. 5(a), reveal higher oxygen contents for samples with higher outgassing. SEM observations show thinner and slanter columnar structure in the AlN film when outgassing is higher upon sputtering. Both of the lower residual stress levels and the lower FWHM values at lower outgassing can be attributed to oxygen-related extended defects [Cherng & Chang, 2008].

Figure 5 © shows the relationship between FWHM and pressure at different target-to-substrate distances. At a longer target-to-substrate distance, the insensitive region shrinks and the threshold value shifts to a lower pressure [Cherng & Chang, 2008]. This is due to the decreasing ratio of mean free path to target-to-substrate distance, indicating more gas phase scattering and thus worse film quality.

With increasing nitrogen concentration, atomic peening is favoured while atom-assisted deposition basically remains unaffected. The former explains the decreasing FWHM values and more compressive stress with increasing N_2 %, as shown in Figs. 6(a) and (b). At a lower base pressure, the influence of atmospheric composition diminishes to such an extent that the FWHM of the rocking curve practically stays the same between 20 and 90 % N_2. This finding, together with the insensitive FWHM vs. pressure regions (see Fig. 6) reveal that oxygen contamination is the most dominant factor for the film properties. In the other hand the residual stress at lower outgassing rates varies little with nitrogen content. The oxygen related extended defects are deductive to compressive stress, instead of tensile stress, which is normally caused by re-sputtering type of defects. As seen in Fig. 6(c), the FWHM of the rocking curve decreases with increasing substrate temperature. This is consistent with the higher mobility of adatoms at higher substrate temperatures. Once again, the behaviour at lower outgassing becomes insensitive with substrate temperature. At this point, it is worth noting that at low outgassing, a somewhat "insensitive" region and/or a so-called "threshold" behaviour exists with all process-related parameters, e.g., working pressure, atmosphere composition, and substrate temperature. This emphasizes the crucial role oxygen contamination plays in pulsed-DC reactive sputtering of AlN thin films.
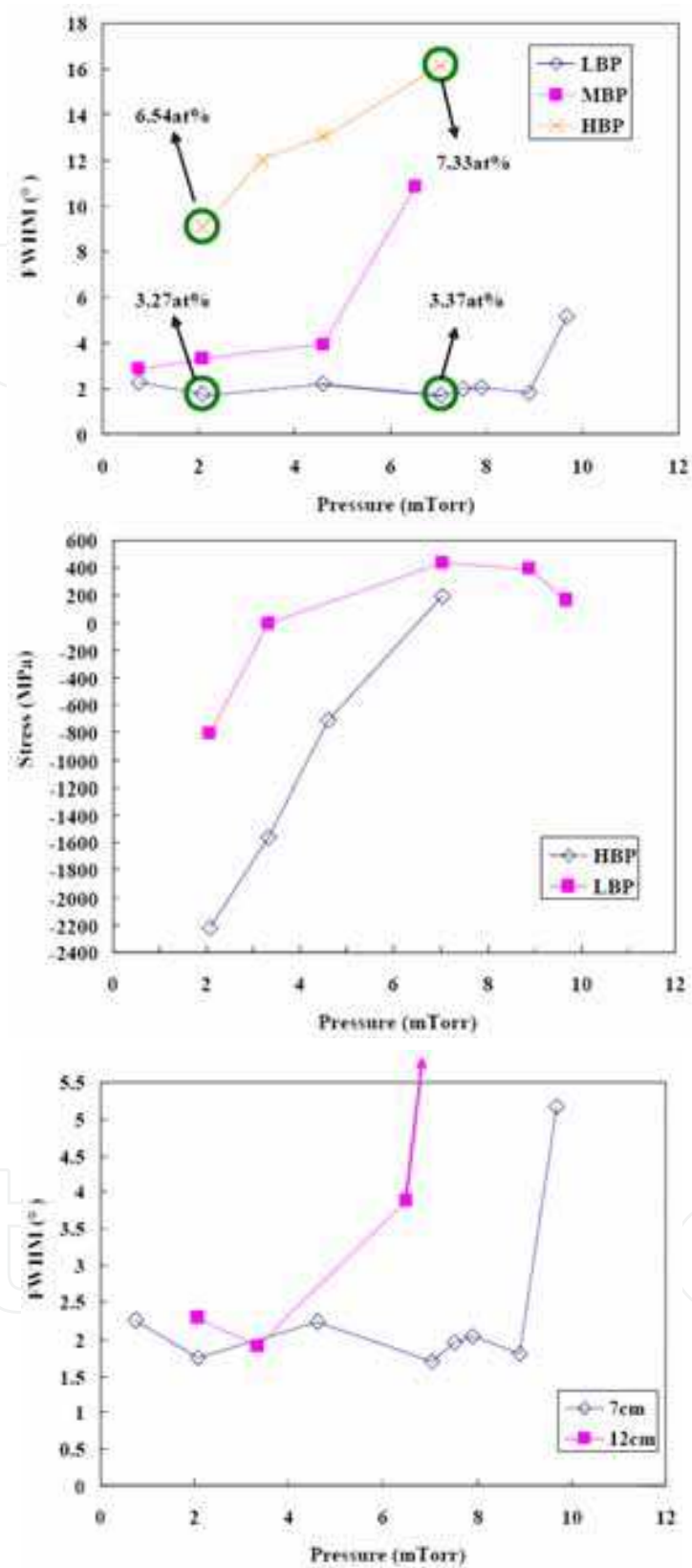
Fig. 5. Effect of working pressure on (a) XRD FWHM; and (b) film stress at various outgassing levels; and (c) on XRD FWHM at various target-to-substrate distances [Cherng et al 2008].
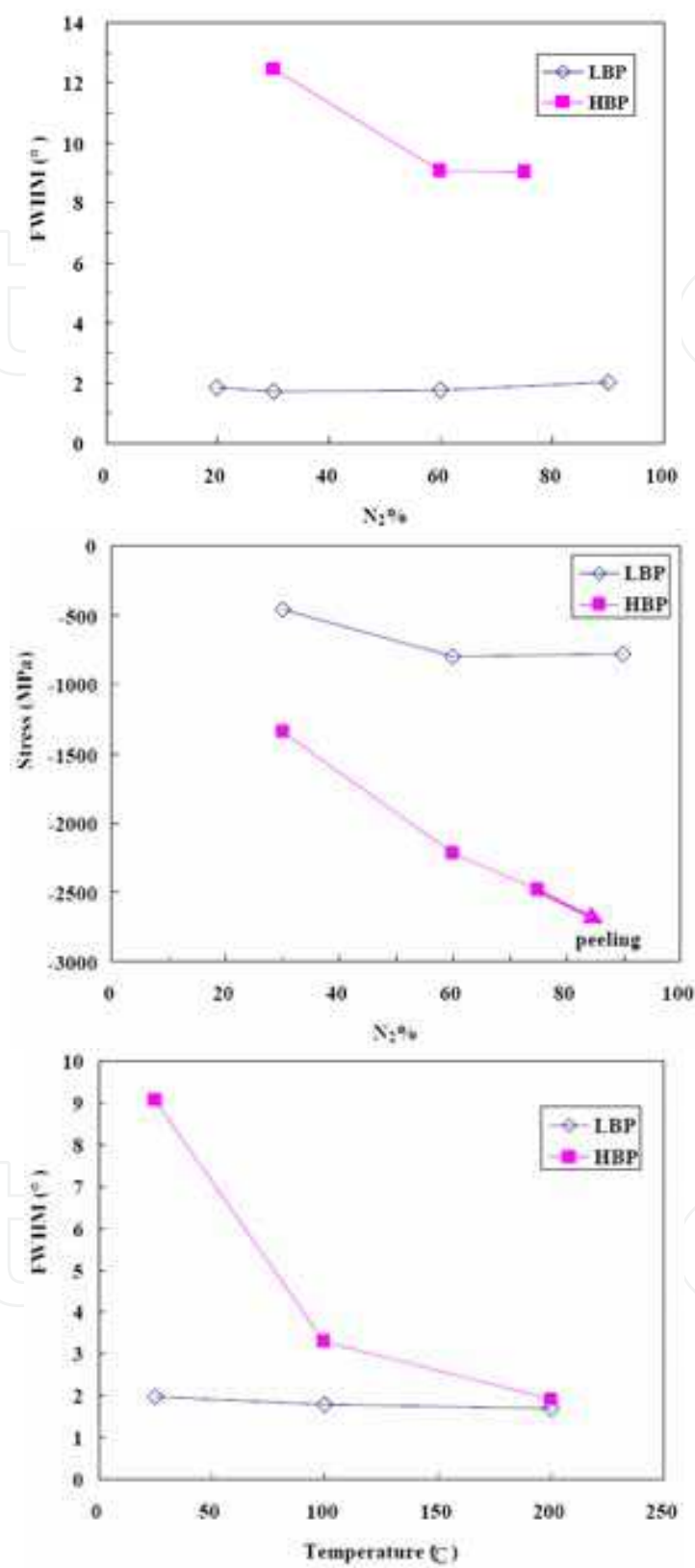
Fig. 6. Effect of atmospheric composition on (a) XRD FWHM (b) residual stress at various outgassing levels; (c) effect of substrate temperature on XRD FWHM at various outgassing levels [Cherng et al 2008].

2.3 Two-step deposition

The growth dynamic or surface kinetic roughening of the sputtered AlN films grown on Si (100) substrates has been thoroughly studied, and a two-stage growth regime identified [Auger et al 2005]. In the first step, the growth dynamic is unstable with significant sticking probabilities of the impinging particles. The films have a mixture of well textured and randomly oriented crystals. In the second regime, the films are homogeneous and well textured, and the growth is dominated by the shadowing effect induced by the bombardment of impinging particles [Auger et al 2005]. Based on this effect, a two-step pulsed-DC reactive sputtering model has been proposed with various process parameters including working pressure, discharge power, and reactive atmosphere during two stage sputtering [Cherng et al 2008, 2009]. Two-step sputtering for an AlN piezoelectric layer generally consists of a 10-min deposition for the base layer and a subsequent 50-min sputter for the top layer. As a comparison, one-step sputtering (60 min) has also been conducted with the same sputter parameters as those used for the base layer in two-step sputtering.

2.3.1 Two-step working pressure method

Figure 7 shows the effects of working pressure on (a) XRD FWHM, and (b) residual stress of AlN piezoelectric layer for both one-step and two-step sputtering, respectively. The data for two-step sputtering, when compared to their one-step counterparts, show a better figure-of-merit in that not only the FWHM of the rocking curve is smaller, but also the magnitude of the residual stress is smaller and its variation with pressure is smoother [Cherng et al 2008]. If we attribute the first step sputtering to initial nucleation and the second step to the subsequent growth of the AlN film, then the better film quality for two-step sputtering (when compared to its one-step counterpart with the same process parameters used for the base layer) has to be due to the sputtering conditions for the growth of the top layer [Cherng et al 2008]. Therefore, as far as the rocking curve width and residual stress are concerned, it is fair to say that growth, instead of nucleation, dominates the performance of two-step working pressure method.

For the AlN film deposited on Mo substrates, the FWHM values for both the 1-step and 2-step methods do not vary with working pressure and remain at the same low value of about 1.3^o as shown in Fig. 7 (a) [Cherng et al 2008]. This is further confirmed by Fig. 7(b), where both the 1-step and 2-step methods using Mo substrates show low residual stress, regardless of the working pressure.

2.3.2 Two-step power method

For one-step sputtering on Si, the FWHM of the rocking curve decreases with increasing discharge power as shown in Fig. 8. This is due to the enhanced atom-assisted deposition and atomic peening mechanisms at a higher power. The sputter yield (at higher discharge voltage) and plasma concentration (more ionized species at higher discharge current) have been increased. Growth, instead of nucleation, dominates the performance of two-step power method on Si, because the data of two-step sputtering are much better than that of its one-step counterpart as also shown in Fig. 8 [Cherng et al 2009].

2.3.3 Two-step nitrogen concentration method

With increasing nitrogen concentration, atomic peening is favoured while atom-assisted deposition remains unaffected. For one-step sputtering on Si, this enhanced atomic peening
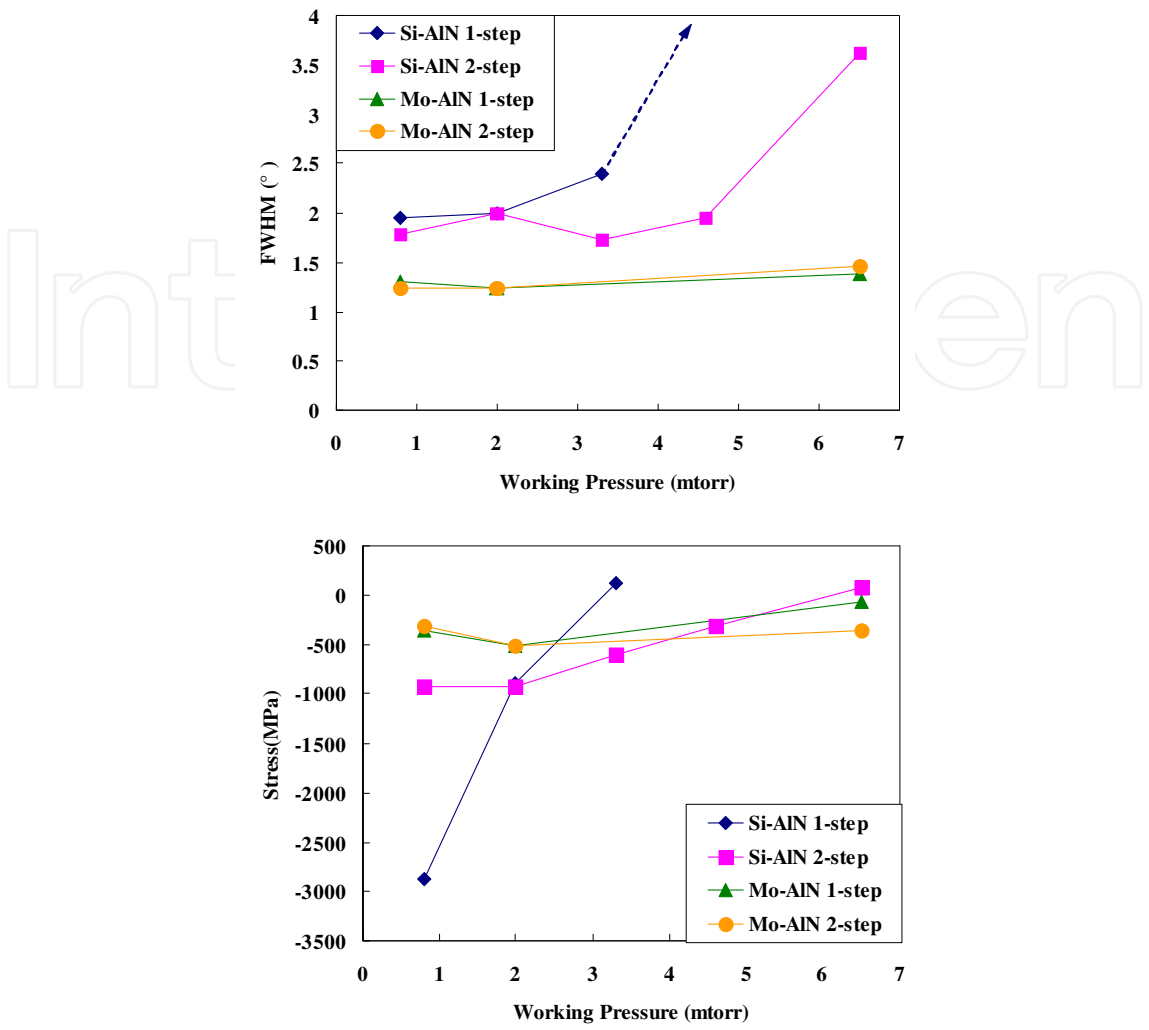
Fig. 7. Effects of working pressure on (a) XRD FWHM, and (b) residual stress of AlN
piezoelectric layer for both one-step and two-step sputtering, respectively [Cherng et al 2008]
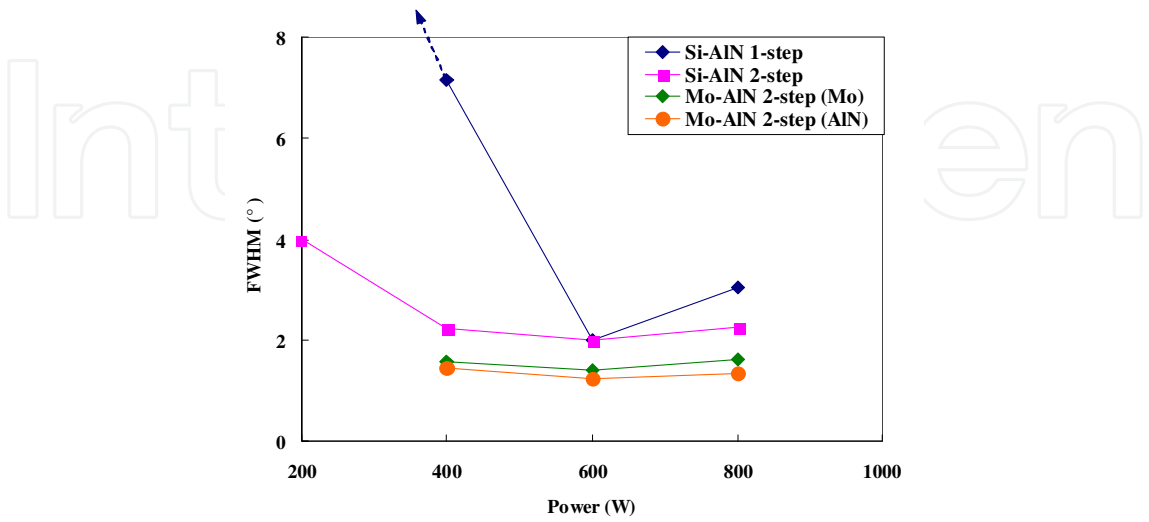

Fig. 8. Effects of discharge power on XRD FWHM for both one-step and two-step sputtering
[Cherng et al 2009].

is thought to be responsible for the decreasing FWHM of the rocking curve from 40 to 60 % of N_2, as shown in Fig. 9. The higher FWHM value at 100 % N_2 is probably due both to the excess atomic peening (causing re-sputtering) and to the worsened sputter yield (since N has a lower sputter yield than Ar). It is worth noting that the target does not exhibit any hysteresis-related phenomenon even under pure nitrogen. The employment of pulsed power is believed to be able to clean up the surface of the Al target effectively [Cherng et al 2009]. On the other hand, the FWHM behaviour for the two-step atmosphere method on Si seems to be mostly determined by initial nucleation rather than subsequent growth. The data for this is much closer to those of the one-step counterparts which employ the same sputtering conditions for the base layer. This phenomenon is just the opposite to the one observed for the other two-step methods described above, and has to be closely related to the atomic peening mechanism. It is thought that in the case of lighter bombarding particles (N atoms for atomic peening vs. Al atoms for atom assisted growth), the sputtering conditions for subsequent growth are not appropriate to alter the effects of the initial nucleation [Cherng et al 2009]. For deposition on Mo, once again, the quality of the AlN piezoelectric film is dominated by the underlying Mo film, regardless of the reactive atmosphere, as evidenced by the two-step sputtering data of the AlN and Mo films.

In conclusion, a methodology of two-step pulsed-DC reactive sputtering has been systematically evaluated for making (0002)-textured AlN thin films with independent control of rocking curve width and residual stress. This methodology was best demonstrated by the two-step working pressure method on Si, which was capable of reactively sputtering AlN thin films with almost constant rocking curve widths of about 2º, with a constant deposition rate of about 36 nm/min, and a continuously adjustable residual stress between −926 and −317 MPa [Cherng et al 2008 and 2009]. In addition, it was noted that growth dominated the performances of both the two step working pressure method and the two-step power method, while nucleation dominated the two-step atmosphere method.
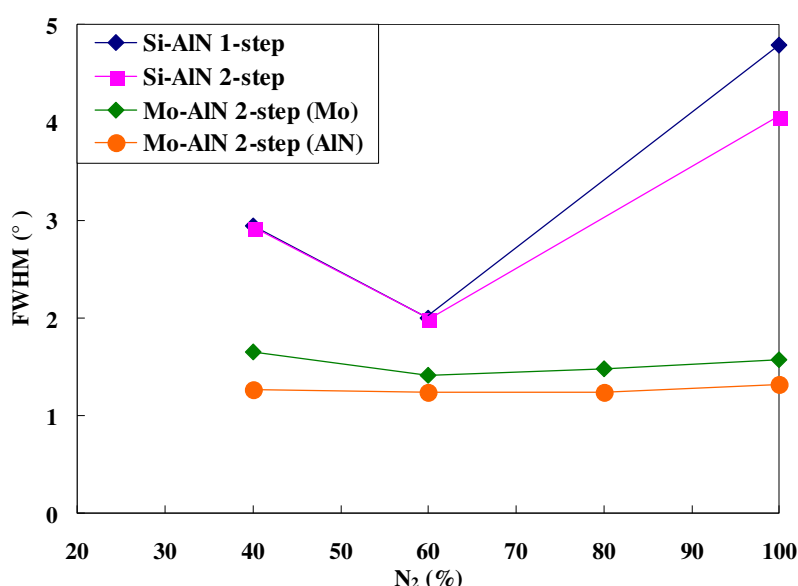

Fig. 9. Effects of reactive atmosphere on XRD FWHM for both one-step and two-step sputtering [Cherng et al 2009].

3. Piezoelectric properties of sputtered AlN films

3.1 Film thickness effect

For a SAW device made on a very thin AlN film (less than a few hundreds of nanometers), the acoustic wave can penetrate much deeper into the substrate as the film thickness is normally much less than one wavelength. In this case, the energy of a SAW device is largely dissipated in the substrate where the wave predominantly propagates. Therefore, the wave velocity of the SAW approaches the Rayleigh velocity of the substrate material as shown in Fig. 10(a) [Clement et al 2003, 2004]. When the AlN film thickness is increased, the acoustic velocity gradually changes to that of AlN film. However, there is normally a cut-off thickness, below which no wave mode can be detected, due to the low electromechanical coupling coefficient for a very thin AlN film. A Rayleigh-type wave (called the fundamental mode or mode 0) can be generated when the film is thin. With increasing film thickness, a higher order acoustic wave mode known as the Sezawa wave (mode 1) can be obtained. A Sezawa mode is realized from a layered structure in which the substrate has a higher acoustic velocity than the overlying film. This wave exhibits a larger phase velocity (higher resonant frequency) than the Rayleigh wave for a fixed thickness, and is thus desirable for high frequency applications. In a similar manner to that of Rayleigh wave, the resonant frequency and the phase velocity of the Sezawa wave decreases with film thickness. There are other higher order acoustic wave modes (modes 2 and 3, etc.) as shown in Fig. 10(a) [Clement et al 2003].

There are two key issues for the piezoelectric properties of the AlN acoustic wave device: the electro-mechanical coupling coefficient k_{eff}^2 and the quality factor Q. The effective coupling coefficient (k_{eff}^2) is related to the relative spacing between the resonant frequency and the parallel resonant frequency, and it determines the bandwidth for a band-pass filters. Fig 10 (b) shows the effective coupling coefficients of different wave modes as a function of the thickness ratio of the electrode-to-piezoelectric layers for AlN thin-film resonators [Clement et al 2003]. The quality factor Q is determined by the energy conversion efficiency from electrical into mechanical energy. However, improving one of those two parameters can cause a decrease of the other one, therefore, it would be necessary to optimize both parameters using one figure of merit (FOM), defined by the product of $k_{eff}^2 \times Q_D$ [Grate 2000].

3.2 Effects of electrodes

For an AlN based acoustic wave device, parameters such as the Q factor, resonant frequency and effective coupling constant are determined by the film and electrode material quality, as well as the electrode thickness and film roughness [Lee et al 2002]. Common used electrode materials include (111) oriented face centered cubic (fcc) metals such as Al, Pt and Ni, (110) oriented body centered (bcc) materials like Mo and W, and hexagonal metals with a (002) orientation including Ti and Ru [Lee et al 2004]. Some commonly used electrode materials for AlN SAW devices include Mo, W, Ti, Al, Au, Pt, Ni and TiN, and Ag, Co, Cr, Cu Fe, Nb, Ni, Zn, Zr have also been reported as electrodes for these acoustic wave devices [Lee et al 2004, Akiyama et al 2004]. Metallic electrodes can help promote the growth of highly *c*-axis oriented AlN films., and they can also contribute to the confinement of the mechanical energy in the piezoelectric layer at the resonant frequency. A high acoustic impedance mismatch between the piezoelectric layer and the electrodes is normally preferred, thus for this purpose, the heavy and stiff metals are the candidates of choice.
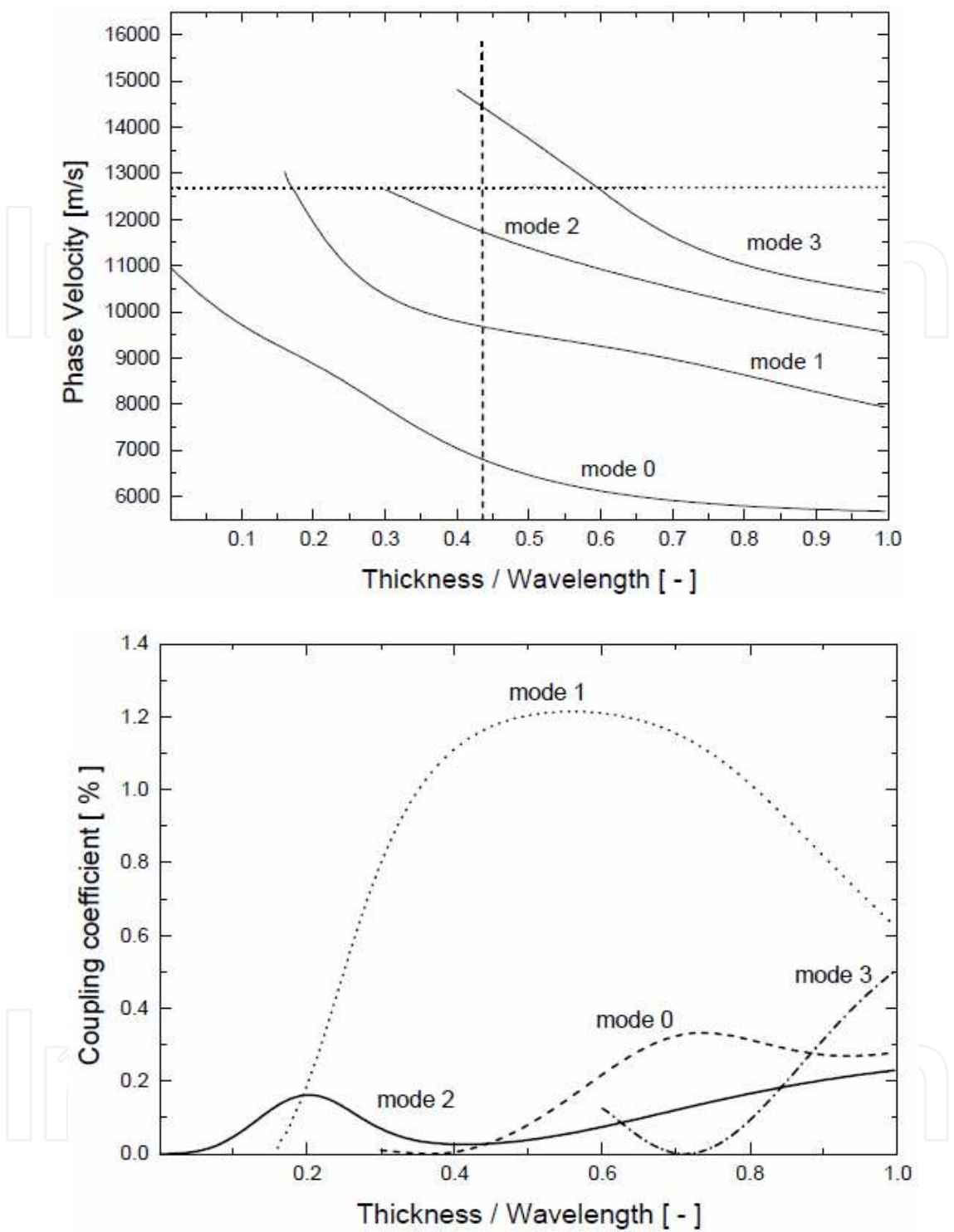
Fig. 10(a). Phase velocity for AlN film as a function of thickness/wavelength ratio for different acoustic wave modes (b). Effective coupling coefficient as a function of thickness ratio of electrode-to-piezoelectric layers for AlN thin-film resonators [Clement et al 2003].

Gold electrodes show the best resonant characteristics. The characteristics of Ag and Cu electrodes are very close to those obtained for gold, but much cheaper. Al and Mo have low resistivity and high Q factors with Mo being one of the most reported electrodes in the AlN film based acoustic devices, because it promotes the growth of highly textured AlN films

[Akiyama et al 2005, Huang et al 2005 a and b, Lee et al 2003, Okamoto et al 2008, Cherng et al 2004]. It was reported that the best-textured AlN films deposited by sputtering on metallic surfaces have been grown on Pt substrates [Lanz & Muralt 2005].

For the AlN FBAR device, the bottom metal layer significantly affects the texture of AlN films and its electro-acoustic properties. AlN films deposited on the materials with fcc lattice structure show a high c-axis orientation, especially for Au and Pt [Tay et al 2005]. Ti has a hexagonal structure similar to that of AlN [Lee et al 2004, Chou et al 2006], while W has a low acoustic attenuation, small mismatch in the coefficient of thermal expansion and high acoustic impedance with AlN, and is thus a good electrode material for AlN devices. Ni has often been chosen because of its surface smoothness, but the AlN film texture on Ni is not as good as that on the other fcc metals. Tantalum [Hirata et al 2007] and iridium [Clement et al 2009] have also been reported as electrodes for AlN film growth. Iridium is of interest as it is a precious metal similar to Pt but considerably cheaper, with a high sound velocity (5300 m/s), and a lower diffusivity in Si than other heavy metals (Au, Pt) [Benda et al 1998]. The thickness ratio of AlN and top or bottom electrodes has been reported to have a significant influence on piezoelectric effect of AlN films [Huang et al 2005 a and b, Akiyama et al 2004]. Lee et al 2002 found that a resonator with a thicker Mo electrode can provide higher Q values than those with thinner Mo electrode.

3.3 Film texture and substrate effect

AlN films with strong texture can have good piezoelectric coefficients, high electromechanical coupling, and acoustic velocities approaching those of the single crystal AlN. The sputtering process parameters significantly affect the orientation of the deposited AlN films. Okano et al. 1992 identified that the c-axis orientation increases as the N_2 concentration in the mixture of Ar and N_2 decreases, while Naik et al 1999 have shown that the c-axis orientation increases as the sputtering pressure is reduced. AlN films have been reported to show preferred (002) growth orientation on a number of materials which include silicon, quartz, glass, $LiNbO_3$ [Caliendo et al 2003, Lee et al 2004], GaAs [Cheng et al 1998], GaN/Sapphire [Kao et al 2008,Xu et al 2006], SiC [Takagaki et al 2002] and ZnO layer [Lim et al 2001]. For AlN film growth, the texture of film is the result of competitive growth of (100) and (001) planes [Clement et al 2003]. When the (001) crystal growth is favourite, the AlN crystals will grow with a (002) orientation. When (100) crystal growth is more favourite, the other orientations can be dominant, such as (103) (100) (110) and (102) etc. The energy input into the plasma adatoms during film growth is the dominant parameter that controls the film orientation. The possible solutions for better orientation include: higher plasma energy, higher Ar ion energy, application of negative self-bias voltage, shorter target-to-substrate distance and lower pressure. [Clement et al 2003].

Sputtered AlN films normally show a (002) film texture, which results in longitudinal (or Rayleigh) wave modes and is therefore good for sensing in air or gas. However, as explained before, if liquid exists on the sensing surface, excessive damping and attenuation of the propagating wave occurs when the longitudinal mode couples into the liquid. This problem can be solved by generating a shear-horizontal (SH) SAW, which propagates on a piezo-material by an in-plane shear horizontal motion [Wingqvist et al 2007], and dramatically reduces SAW coupling into a liquid medium [Mchale 2003]. However, the commonly observed (002) texture in the sputtered AlN films is unsuitable for generating SH–SAWs. In addition, using a pure shear wave is not efficient for driving liquid droplets forward. A good approach to solving the problem is to develop AlN films in which the c-

axis is inclined relative to the surface normal, thus allowing both longitudinal and shear wave modes to be generated [Webber 2006]. These two modes will have different frequencies and thus can be individually controlled for either pumping or sensing purposes. To the best of our knowledge, there are no reports of the application of both the functions (microfluidics and biosensing) on a c-axis inclined AlN based SAW device in liquid conditions. The techniques for the deposition of the inclined AlN film include: (1) using a tilted substrate (up to 45°) with a controlled position under the sputter-target; (2) using a high energy nitrogen ion beam aimed at the desired angle with respect to the substrate surface normal [Yanagitani & Kiuchi 2007]. Obtaining the inclined AlN films strongly depends on the sputtering pressure, temperature, the oblique incidence of particles [Yang et al 2009]. C-axis inclined AlN films have been deposited on different substrates, including silicon and diamond [Fardeheb-Mammeri et al 2008]. Bjurstrom et al 2004 systematically studied the electromechanical coupling coefficient for both the shear and longitudinal modes at different AlN inclined angles. The k^2 of longitudinal mode has a maximum value for C-axis AlN crystals (θ=0°), but gradually decreases as angle increases. On the contrary, the k^2 value of shear mode gradually increases as the inclined angle is increased from 0 to a peak value at angle of 45°. The k^2 value of the two modes reaches to a similar value at angle of 30 to 35° [Bjurstrom et al 2004].

The acoustic velocity in an AlN/Si SAW device also depends on the orientation of the Si substrate, being about 4700 m/s for Si (111) and 5100 m/s for Si (100) [Clement 2003]. AlN films have been deposited on 128° LiNbO$_3$ substrate in order to enhance the SAW velocity and improve the temperature stability, i.e., decrease the temperature coefficient of frequency (TCF) [Kao et al 2003, Wu et al 2001 and 2002].

Recently, there has been much research on the deposition of AlN on diamond for SAW devices [Mortet et al 2003, Kirsch et al 2006, Le Brizoual et al 2007, Paci et al 2007, Elmazria et al 2003 and 2009, El Hakiki et al 2007, Wu et al 2009, Shih et al 2009, Iriarte et al 2003, Benedic et al 2008, Lin et al 2009]. The drive for this is that diamond substrates offer a higher phase velocities (6 km/s to 16 km/s) [Wu et al 2008]. Figure 12 shows dispersion curves of the first five Rayleigh SAW modes of IDT/(002) AlN/(111) diamond devices plotted as a function of the film thickness ratio h/λ. The phase velocity of each mode decreases as the film thickness ratio increases. For mode 0, the value of phase velocity is determined by the SAW velocity of (111) diamond, i.e., 10.9 km/s at h/λ =0 and the film thickness ratio h/λ increases, the phase velocity rapidly decreases. At h/λ =3, the velocity of the (002) AlN/diamond is about 5.4 km/s. It can be observed that the harmonic peaks of modes 1, 2, 3, and 4 cut off at the critical point where the phase velocity is equal to the shear bulk wave velocity in (111) diamond (12.3 km/s). For example, the cut-off of mode 1 occurs at h/λ= 0.172, mode 2 at h/λ =0.295, mode 3 at h/λ= 0.594, and mode 4 at h/λ=0.693 [Wu et al 2008]. Similar results have been reported by Benetti et al 2005.

The formation process and growth mechanism of an AlN layer on a (001) diamond substrate has been studied by Imura M et al, 2010. At the initial stage of AlN growth on diamond, the randomly oriented AlN grains are generated and grown three dimensionally with the formation of columnar domains due to the 20% lattice mismatch between AlN and diamond. At the second stage of growth, the c-axis-oriented AlN grain grows by incorporating the randomly oriented AlN grains. This occurs because of the high-growth rate of AlN grains along the [0001] direction [Imura M et al, 2010]. Diamond is a better substrate for epitaxial AlN growth than Si (111) [Imura M et al, 2010], but it is expensive, needs to be deposited at a high temperature, and the resulting surface roughness of the

diamond film is normally quite high. Other alternative choices are diamond-like-carbon (DLC) and nanocrystalline diamond films.
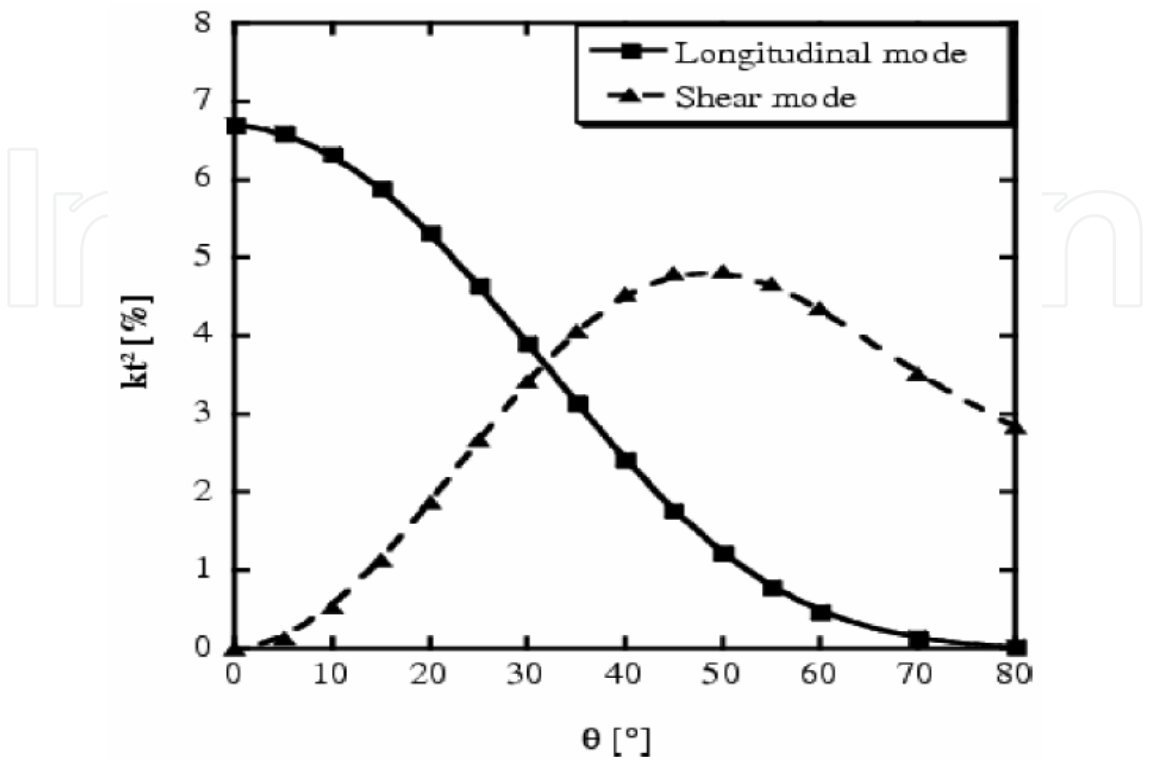

Fig. 11. Electromechanical coupling for both shear and longitudinal modes at different AlN crystal tilt, θ [Bjurstrom et al 2004]
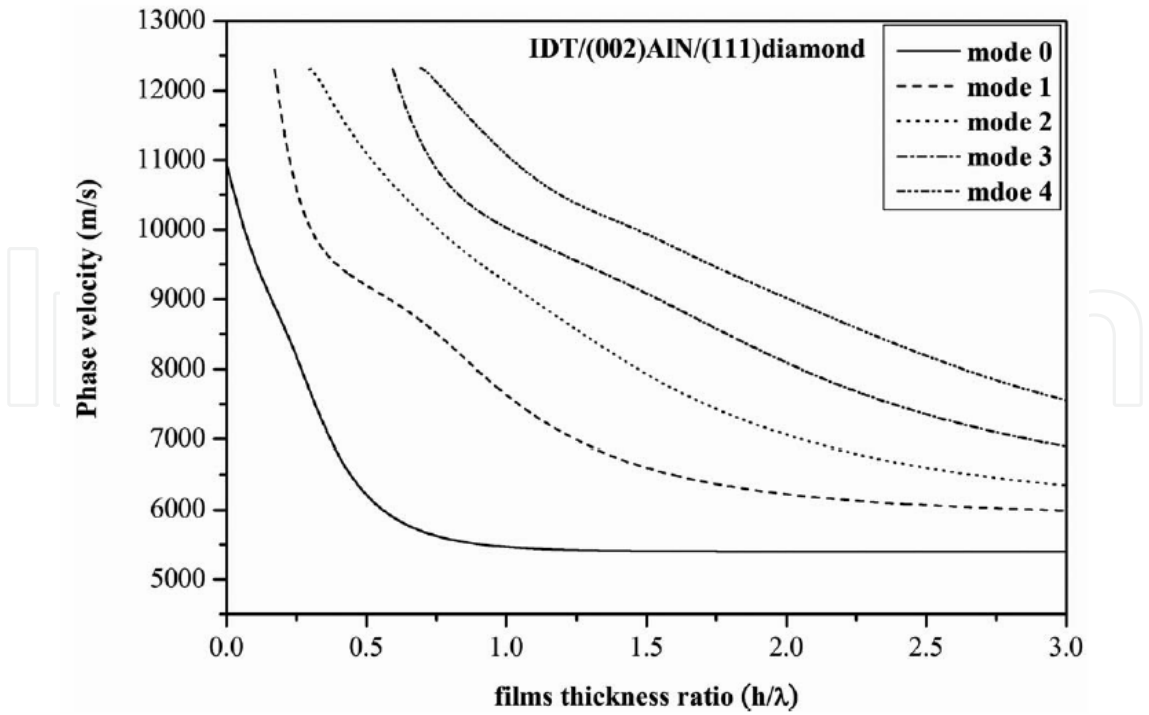

Fig. 12. Phase velocities dispersion curves of the first five Rayleigh SAW modes propagation in the IDT/(002)AlN/(111)diamond [Wu et al 2008].

Recently, AlN has been grown on SiC/Si substrate at a relatively low cost. The CTE of the SiC closely matches that of AlN, and the lattice mismatch is less than 1%. Both materials have been used in applications in high temperature packaging, and AlN thin films have been used as buffer layers for SiC grown on Si substrate [Chung & Kim 2007]. Therefore, SiC is an ideal candidates for a buffer layer of AlN films grown on SiO_2/Si substrates for SAW applications at different temperatures [Hoang & Chung et al 2009].

The AlN's temperature dependent ultrasonic properties (including ultrasonic attenuation coefficient, ultrasonic velocity, and acoustic coupling coefficient constant) have been calculated in the temperature range 200 to 800K by Pandey & Yadav 2009. The total attenuation is mainly dominated by phonon-phonon interaction, and the attenuation decreases from 200– 400 K sharply but it increases gradually from 400–800 K. Thus the temperature 400 K is the characteristic temperature for AlN. The decrease in attenuation from 200–400 K is due to the temperature variation of the thermal relaxation time or thermal conductivity of the material [Pandey & Yadav 2009]. A gradual increase in the attenuation from 400–800 K correlates mainly the temperature variation of the ultrasonic velocities or second order elastic constants. The temperature dependent ultrasonic velocity gives direct information about temperature variation of elastic constants, and the ultrasonic attenuation directly relates to the thermal conductivity or thermal relaxation time at temperature below 400 K and the elastic constants/ velocity of AlN above 400 K [Pandey & Yadav 2009]

During sputtering, particle bombardment can induce large film stress [Iborra et al 2004], and films with large compressive stress can cause buckling–induced delamination in the deposited films and fracture in the released devices. In Ar/N_2 based deposition system for AlN film, the energy of Ar ions colliding with the substrate controls the preferred orientation of the AlN films. The direction and energy of the ions determine the residual stress levels of the AlN films. The film stress or energy of the Ar bombardment can be adjusted by the substrate bias voltage during sputter deposition. Thermal annealing is a good method for post-treatment to reduce the film stress and improve the coating quality [Hung & Chung 2009].

4. MEMS processing and functionalization of AlN films

There are some reports on surface micromachining of AlN [Hara et al 2005], and chromium has been used to form both a good etch mask and electrode [Saravanan et al 2006]. Germanium can be used as the sacrificial layer for the AlN films, instead of common amorphous silicon, SiO_2, or other metal layer. AlN can be etched in aqueous solutions, such as KOH, NaOH, HF/H_2O, HF/HNO_3, tetramethyl ammonium hydroxide (TMAH), and the etch rate is temperature and crystal polarity sensitive [Jasinki et al 2003, Sheng et al 1988, Tan et al 1995]. Dilutate TMAH etches AlN but when with silicic acid and ammonium persulphate, it can be used to etch silicon with a very low etch rate for AlN film, and thus can be used for sacrificial etching [Kar et al 2009]. AlN can be electrochemically etched in electrolytes, such as HPO_3 (60^oC to 90^oC) or KOH solutions, and the etch rate is strongly dependent on the coating quality (from tens of nm/min up to a few μm/min). The reaction can be expressed as [Zhang & Edgar 2005]:

$$AlN + 6KOH \rightarrow Al(OH)_3 \downarrow + NH_3 \uparrow + 3K_2O \downarrow \qquad (5)$$
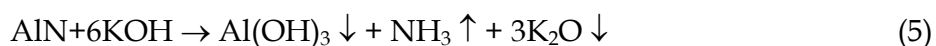
For dry etching process, AlN is normally etched using chlorine based plasma, such as chlorine and BCl₃, rather than a fluorine, as aluminum fluoride is stable and non-volatile [Khan et al 2002 or 2006]. Etching in a Cl-based plasma is normally isotropic, and the volatile reaction product is $AlCl_3$ at high temperatures (above 180ºC) or Al_2Cl_6 at a room temperature [Engelmark 2003].
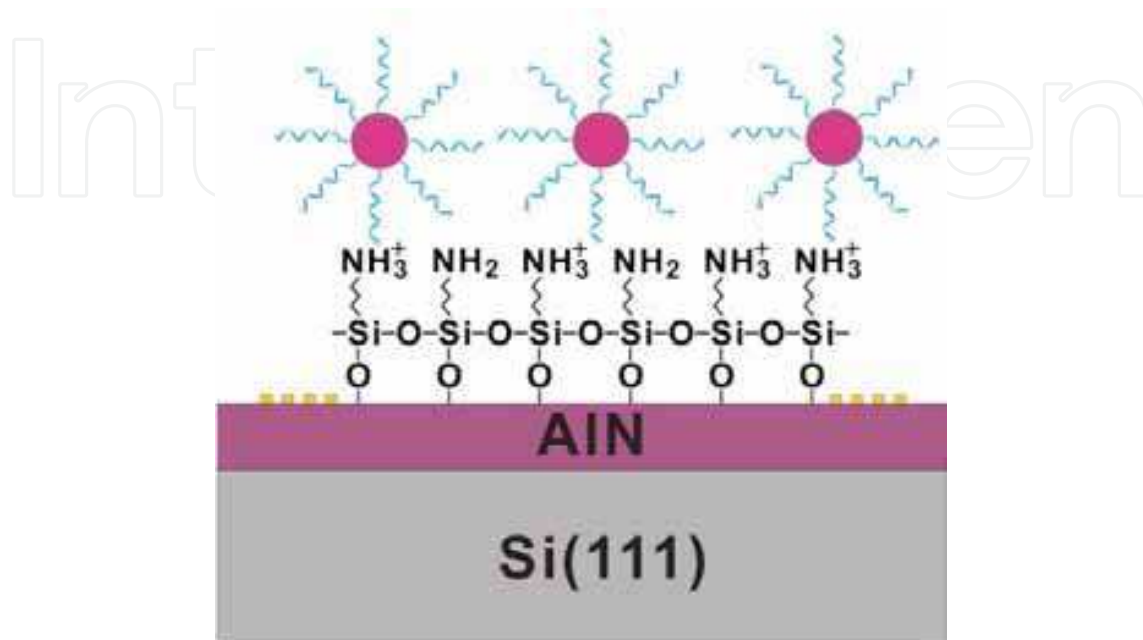

Fig. 13. Schematic diagram of antibody immobilized AlN/sapphire [Chiu et al 2008]

Recently, there have been studies for the surface functionalisation of AlN film for biosensing applications [Chiu et al 2008]. For example, by using silane, a new chemical layer can form on the AlN, and the functional groups on the silane surface can then be used as anchor points for the antibodies. In reference [Chiu et al 2008], antibody immobilized AlN/sapphire was prepared using the process shown schematically in Fig. 13. The AlN films were pre-treated prior to silanization using two methods. In the first method, they were treated by exposure to oxygen plasma. The second method treated the AlN surfaces by ultrasonication in 3/1 (in vol%) piranha solution, followed by rinsing in DI water. Piranha treatment was chosen because it is commonly used as a surface preparation method for silanization of other types of inorganic surfaces. Improved silane surfaces should create a more stable and ordered silane layer for the linkage of antibody, phage or other detecting ligands in the biosensor under development [Chiu et al 2008]. The treated AlN samples were silanized with octadecyltrichlorosilane (OTS). The ability to produce repeatable, homogeneous layers of selected chemical groups by silane derivatization of the AlN surface is considered to be a promising step in the development of a biosensor that uses surface immobilized phage or antibody ligands for analyte detection [Chiu et al 2008].

5. Thin film acoustic devices for biosensor applications

5.1 AlN SAW device

AlN based SAW devices have been reported as promising for high frequency, high sensitivity applications [Chiu etal 2008, Caliendo 2003 a and b, Xu et al 2004, Assouar et al

2002, Mortet et al 2003, Clement at al 2004]. For example, AlN Rayleigh SAW device with velocity of 4590 m/s has been fabricated for surface biofunctionalization using amiosilane molecules as cross-linker to form a monolayer of DNA-Au particle [Chiu etal 2008]. Electrostatic interaction between the positively charged surface amine groups and negatively charged DNA-Au nanoparticle conjugates allows the self-assembly of a probe nanoparticle monolayer onto the functionalized AlN surfaces under physiological conditions. Results showed that Au nanoparticles can play multiple roles in SAW sensing for probe molecule immobilization, signal amplification, and labelling [Chiu et al 2008].

The substrate can have a significant effect on the acoustic velocities of the AlN SAW devices. For example, Clement et al 2007 have reported that SAW velocity depends on the orientation of Si wafers (4700 m/s for Si (111) and 5100 m/s for Si (100)). AlN films deposited on a LiNbO$_3$ substrate have been reported to form a highly sensitive Love mode sensing device [Kao et al 2003 and 2004]. To increase the operating frequency, it is common to use substrate materials with high acoustic velocities, including sapphire, SiC, diamond, etc. Assouar et al 2002 reported a SAW device on a sapphire substrate, which achieved a velocity of 5536 m/s, compared with 5055 m/s measured on a silicon substrate. The acoustic wave velocity associated with sapphire is very close to that of AlN, which limits the acoustic velocity dispersion. AlN/sapphire is hence an attractive structure for SAW devices operating at very high temperature and high frequency applications in harsh conditions [Aubert et al 2010]. Takagaki et al 2002 fabricated AlN SAW devices on SiC substrates, with a higher-order Rayleigh mode and a frequency of 19.5 GHz, corresponding to a velocity above 7000 m/s. Benetti et al 2005 fabricated (002) AlN/diamond/Si SAW devices, with a velocity of 8200 m/s for Rayleigh mode waves and 10784 m/s for Sezawa mode waves.

SH-SAW has been generated using AlN film with laser micromachined grooves [Xu et al 2004]. This required the formation of grooves with periodicity smaller than half the wavelength of the SAW, thus the longitudinal waves is damped and only the SH-SAW can propagate. The so-formed SH-SAW can be used in a liquid biofludic system without significant signal loss, with a high mass sensitivity of 1.35 ng/ml (Xu et al 2004). However, the process is complicated as it needs precision laser microprocessing of the groove.

5.2 Lamb wave devices

In a manner similar to a SAW device, Lamb wave devices on a membrane structure have been used for biosensing in liquid [Muralt et al 2005]. The wave velocity generated in the Lamb wave is much smaller than those in liquids. This minimizes the dissipation of wave energy into the liquid, thus the Lamb wave sensors can be used in a liquid environment [Wenzel & White 1990, Nguyen & White 2000]. The detection mechanism is based on the relative change in magnitude induced by the perturbation on the membrane, and not on the resonant frequency shift. Therefore the sensitivity of these devices increases as the membrane thickness becomes thinner. Lamb wave devices utilizing the lowest order symmetric Lamb wave (S0) propagating in a highly textured 2 μm thick AlN membrane has been successfully demonstrated by Yantchev and Katardjiev in 2007. AlN based Lamb wave resonators can have very high acoustic velocity, up to 10,000 m/s using the lowest symmetric (S0 mode) Lamb wave device, which also shows a low dispersive characteristic [Ling et al 2010]. The main drawback of the Lamb wave biosensor is that there is a practical limit on the minimum film thickness as the thin film becomes more fragile.

Duhamel et al (2006) prepared an AlN/Si based Lamb wave biosensor, and obtained a sensitivity of 200 cm²/g. However, due to the thin membrane structure, the temperature

sensitivity is also significant as the AlN/Si Lamb wave device has a non-zero temperature coefficient of frequency (TCF) in the range −20 to −25 ppm/°C [Wingqvist et al 2009]. Therefore, temperature compensation is normally necessary. Different types of temperature compensation methodology have been proposed for AlN Lamb wave devices [Zuo et al 2010, Lin et al 2010, and Wingqvist et al 2009]. For example, AlN was deposited on P+ doped silicon (which has a positive TCF of 9 ppm/K) to compensate the temperature effect. The most reported method is to use AlN/SiO$_2$ composite layer structure (as SiO$_2$ has a TCF of 85 ppm/K) [Bjurstorm et al 2007, Lin et al 2010]. The Lamb wave resonators with almost zero TCF have been fabricated using a composite AlN/SiO$_2$ membrane structure with different AlN/SiO$_2$ thicknesses (see Fig. 14) [Wingqvist et al 2009], with a Q factors of around 1400 at a frequency of around 755 MHz.
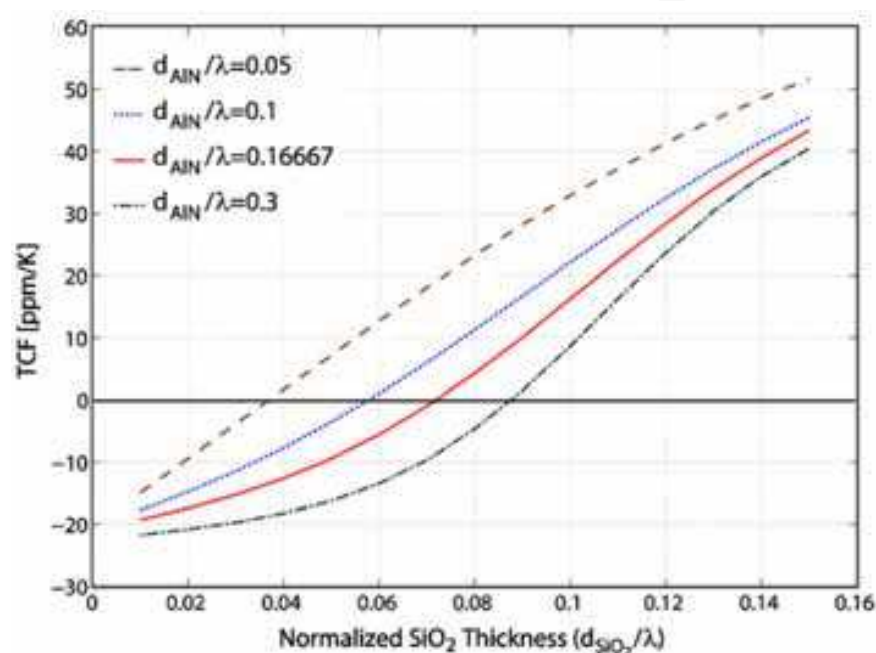
Fig. 14. Temperature coefficient of frequency as a function of the SiO$_2$ thickness for AlN plates of varying thicknesses normalized to the wavelength (λ) [G. Wingqvist et al, 2009-b]

5.3 AlN FBAR device

Probably, the most of common AlN based acoustic wave biosensor is FBAR structure. Similar to the QCM, an FBAR device (shown in Fig. 16a) consists of a submicron thick piezoelectric film membrane sandwiched between two metallic electrodes [Ruby 2007, Benetti 2005]. The frequency shift Δf due to mass loading Δm of an acoustic wave device can be calculated by [Buttry & Ward 1992]

$$\Delta f = \frac{2\Delta m f_o^2}{A\sqrt{\rho\mu}} \tag{2}$$

where A, ρ, μ and f_o are the area, density, shear modulus and intrinsic resonant frequency, respectively. Owing to the much reduced thickness, the FBAR device operates at high frequencies, up to a few GHz, and the attachment of a small target mass can cause a large frequency shift – typically a few MHz. This makes the signal easily detected using simple

electronic circuitry. Figure 15 summarizes the sensitivity range for different types of resonators according to their normal operational frequency ranges [Rey-Mermet at al 2004]. The advantages of the FBAR device includes: (1) the ability to fabricate the device using standard CMOS processing and compatible materials allowing integration with CMOS control circuitry; (2) the significantly reduced size and sample volume. These features together with the intrinsic high sensitivity make the FBAR devices ideal for highly sensitive real time diagnostic biosensor arrays, which provide quantitative results at a competitive cost. However, for the membrane based FBAR design, the membrane fragility and the difficulty in its manufacture are significant issues which have yet to be fully addressed.
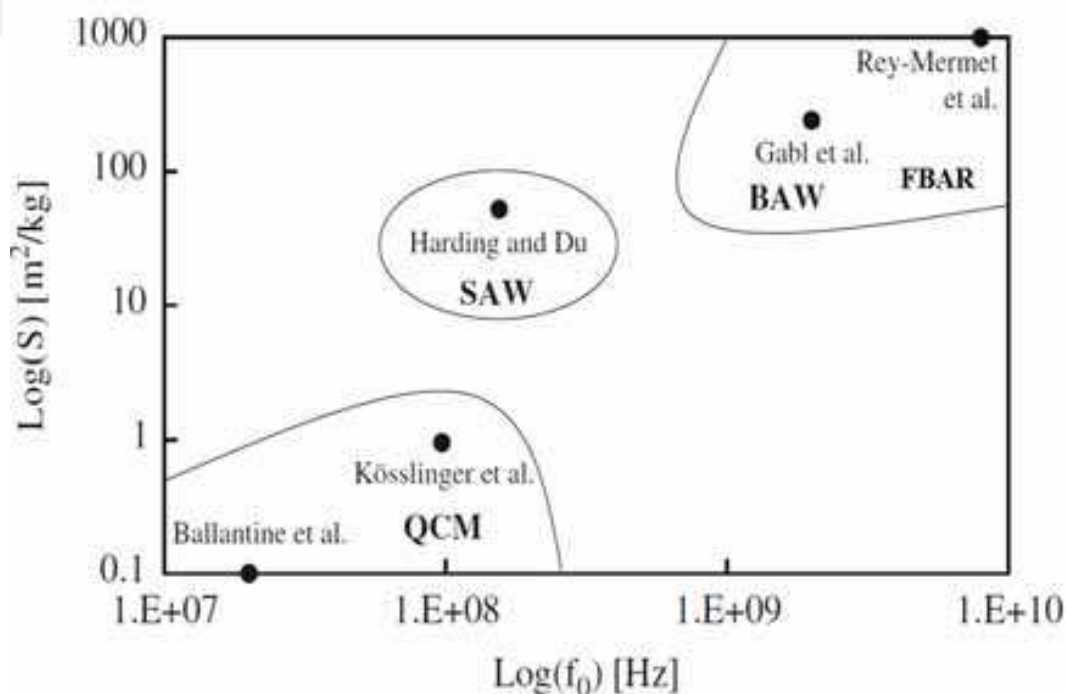
Fig. 15. Sensitivity range for different types of resonators according to their common applied frequency ranges (Rey-Mermet at al 2004)

In addition to the membrane based FBAR structure, there is another common FBAR structure that uses an acoustic mirror deposited between the piezoelectric layer and the substrate (see Fig. 16b). The acoustic mirror is composed of many quarter-wavelength layers of alternating high and low acoustic impedance layers. Due to the high impedance ratio of the acoustic mirror, the acoustic energy is reflected and confined inside the top piezoelectric layer, thus maintaining an excellent resonant bandwidth. This design has a better mechanical robustness and a simpler process control compared with the membrane-based structures. Also cheap substrates, such as glass or plastics can be used, thus the cost can be reduced. Disadvantages for this type of FBAR design is that the process requires thickness and stress control for each layer, increasing the number of the fabrication steps.

There is a third FBAR design which uses a front side etching process [Kang et al 2005]. Initially a sacrificial layer is deposited on the substrate followed by the electrodes and the piezoelectric film depositions. The release of the structure from the substrate is through an air gap made by reactive ion etching of the sacrificial layer. The required selectivity control during the etching process is critical during the fabrication. One disadvantage is the potential liquid trapping inside the gap during biodetection.

An AlN FBAR device has been first reported by Latin et al 1981, and has already been successfully commercialized in the communication industry [Kim et al 2001, Tadigadapa et al 2009], and has also been used as chemical or gas sensors [Benetti, et al 2005]. FBAR biosensors have recently attracted great attention due to their inherent advantages compared with SAW and QCM biosensors: high sensitivity, low insertion loss, high power handling capability and small size [Bjurstrom et al 2004, Kang et al 2005, Loebl et al 2003, Chiu 2007 and 2008]. AlN based FBAR devices have been used to detect carcioembryonic antigen (cEA), a type of glycoprotein associated with breast, colorectal and lung cancer, and the fabricated FBAR device has a frequency of 2.477 GHz, and a sensitivity of 3514 Hz cm^2/ng [Lee et al 2010]. For FBAR, the thickness of the piezoelectric film AlN is comparable with that of the electrode, or bottom layer, being similar to SiO_2 or Si_3N_4. Therefore, the materials for the electrodes and their thickness can influence significantly the performance of the FBAR device.
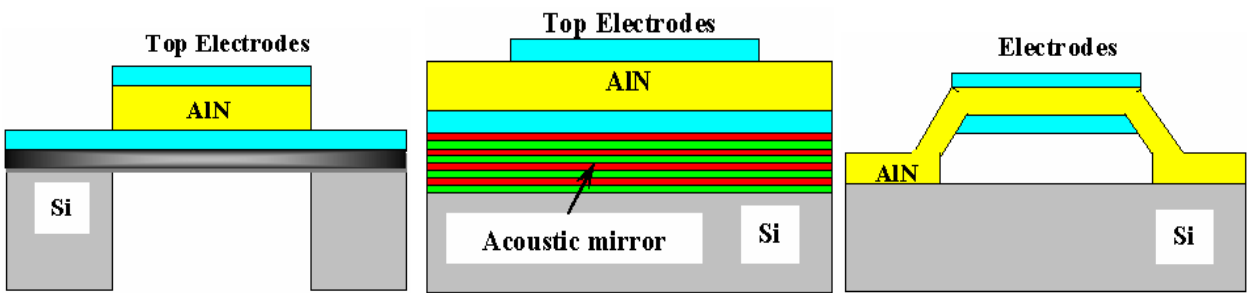
Fig. 16. Types of FBAR resonators: (a) membrane FBAR, (b) air gap FBAR and (c) solid mounted resonator.

For liquid FBAR sensing, there is good reason to deposit an AlN film in which the *c*-axis is inclined relative to the surface normal, thus allowing both longitudinal and shear wave modes to be generated [Weber 2006]. Wingqvist et al. 2007 have fabricated a biochemical sensor based on inclined c-axis AlN for cocaine and heroin detection (see Fig. 17). The FBAR sensor was tested in an immunoassay using avidin/antiavidin detection with a sensitivity of 800 Hz cm^2/ng [Wingqvist et al. 2007]. However, the quality factors was low (100 to 150 for FBAR and 2,000 for QCM) and noise level high, thus the overall detection limit of FBAR is not as good as for QCM devices (detection limit of FBAR was twice as much for a commercial QCM) [Wingqvist et al. 2007]. Wingqvist et al 2009 also used shear mode FBAR devices for multilayer protein sensing, i.e., alternating layers of streptavidin and biotinated BAS, as well as cross-linking of fibrinogen with EDC activation of its carboxyl groups.
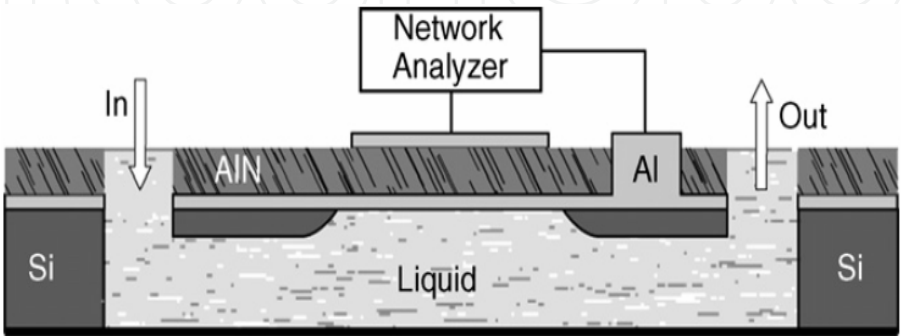

Fig. 17. Schematic picture of lateral FBAR structure comprising the resonator with two electrodes solidly mounted on an acoustic Bragg mirror (from Wingqvist et al 2007a,b)

Another popular method to use FBAR devices in liquid solution is to use lateral field excitation (LFE) of the piezoelectric layer. This requires both signal and ground electrodes being in-plane and parallel on the exposed surface of the AlN film (as can be seen by comparing the conventional longitudinal FBAR electrode design and LFE FBAR design in Fig. 18). A laterally excited AlN thickness shear mode resonator is extremely simple to fabricate and highly sensitive to surface perturbations. The resonator configuration consists of a laterally excited, solidly mounted AlN thin film resonator and the device has been reported to operate stably in biologically equivalent environments such as NaCl in deionized water [Dickherber et al 2008, Corso et al 2007, 2008].

(a)	(b)
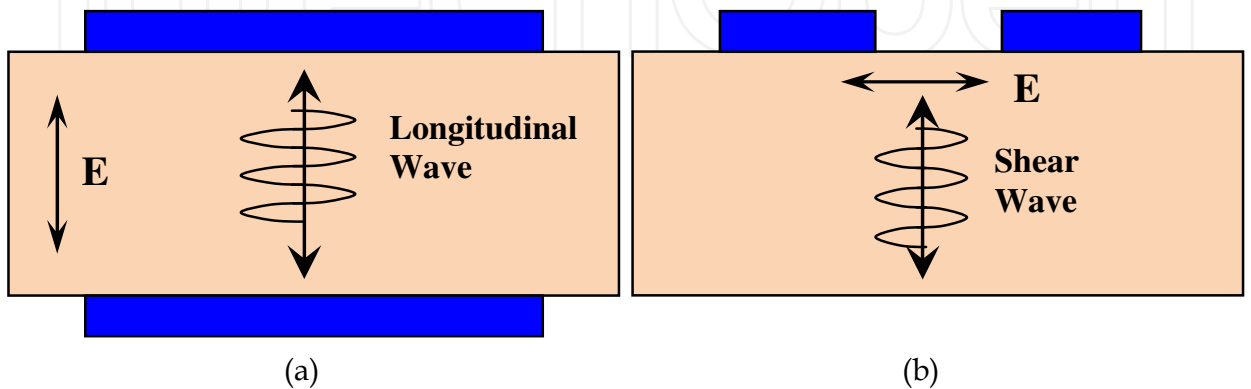
Fig. 18. Comparison of (a) the conventional longitudinal FBAR electrode design; and (b) LFE FBAR design

Xu et al 2010 have proposed a new FBAR of high quality factors Qs operating in liquid media. The FBAR is made of a suspended circular shaped AlN ring sandwiched between the top and bottom Au electrodes, which can be excited in a contour mode (Fig. 19). By exciting in its radial-extensional mode, the resonator experiences the shear viscous damping instead of the squeeze damping, which significantly alleviates the acoustic energy dissipated in the contacting liquid. By having a low motional resistance or coupling with liquids, the contour mode FBAR achieved Qs up to 189, which is more than 13-19 times than conventional FBAR device in liquids and the resonator was used to test an aptamer—thrombin binding pair, with a mass resolution of 1.78 ng cm² [Xu et al 2010].
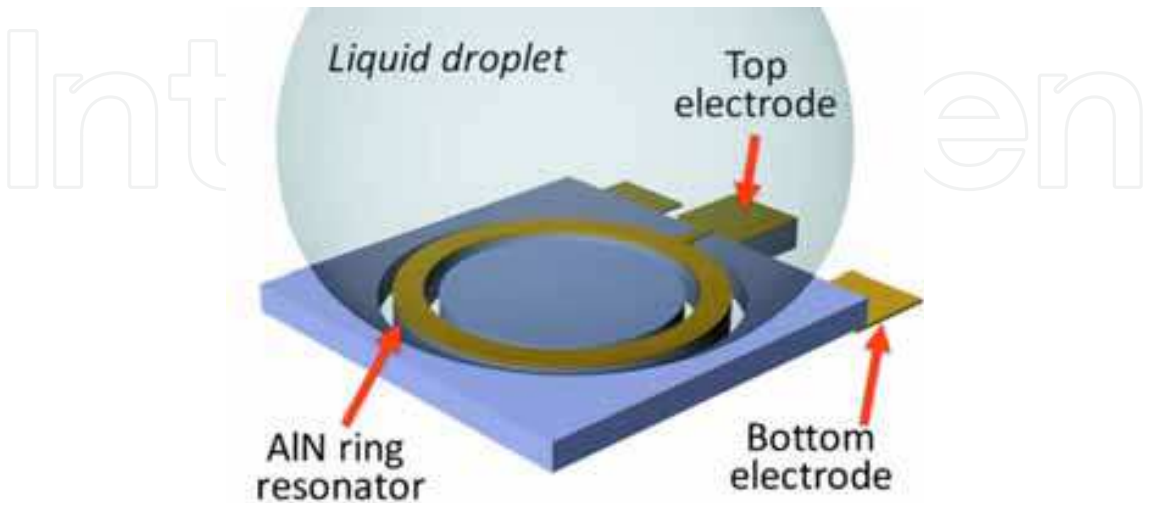

Fig. 19. Schematic figure of the contour-mode AlN FBAR biosensor contacting with a liquid droplet [Xu et al 2010]

Although FBAR based biosensor exhibit a high sensitivity and good resolution, there are some issues to be addressed. For example, they normally have high acoustic wave attenuation and low quality factor due to potential thin film material defects and thin membranes. Other issues include the sensor packaging and the effect of high frequency on biochemistry [Wingquist et al 2007 a and b]. Zhang & Kim 2005 have reported that the second harmonic mode of wave can be excited at a frequency about twice of the fundamental resonance, thus the FBAR using the second harmonic longitudinal mode can have a high Q factor and a low dissipation of acoustic energy into the liquid. Similar to Lamb wave device, the temperature stability of the FBAR is a critical issue, and a composite layer of AlN/SiO$_2$ is a common method that can be employed to compensate for the temperature effect.

6. AlN film for microfluidic applications

In an AlN based SAW device, the interaction between the longitudinal acoustic wave and liquid droplets can be used to create acoustic streaming which can establish a stable streaming pattern with a double vortex (see Fig. 20). This SAW streaming induces an efficient mixing and agitation within the droplets, which can be utilised to produce good micromixers [Fu et al 2007, Fu et al 2010]. When an RF voltage is applied to the IDTs on a piezoelectric film, the water droplet becomes deformed from its original shape (following the Rayleigh angle) with an increased leading edge and a decreased trailing edge contact angle. After surface hydrophobic treatment, the liquid droplets can be pumped forward, with the droplet movement being a combination of rolling and sliding, which is also dependent upon the power applied and the droplet size.
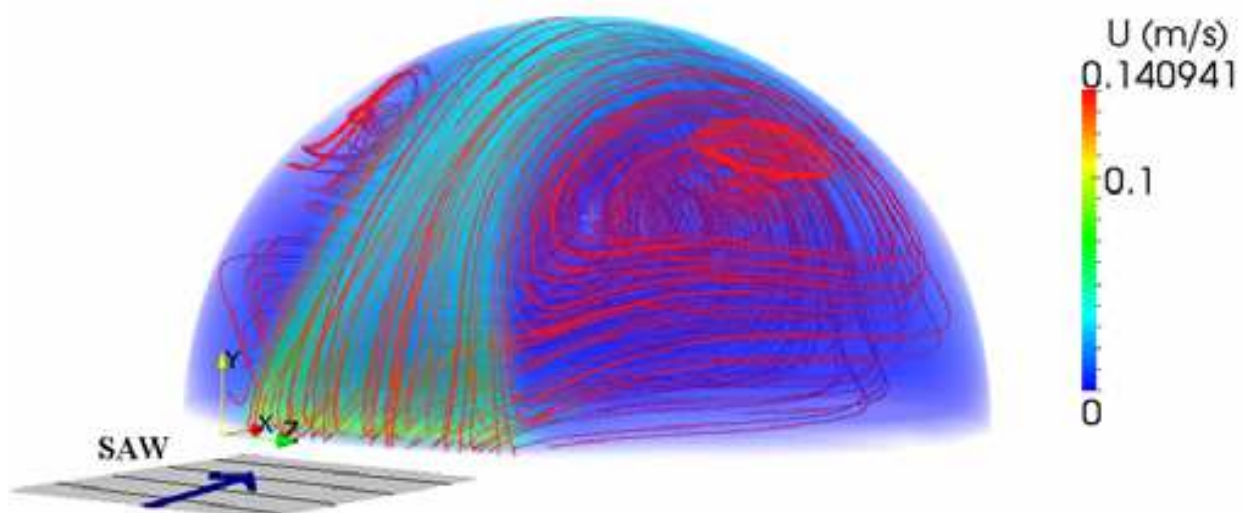

Fig. 20. Numerical 3D illustration showing the droplet SAW interaction leading to 3D complex flow patterns due to SAW energy attenuation and Reynolds stresses formation which in turn producing effective steady force acting in the fluid body "(Courtesy from Mr. Alghane Mansuor)

When the RF power applied to the IDT of an AlN SAW device is sufficiently high, tiny liquid droplets will be ejected from the surface. Ejection of small particles and liquid has many applications ranging from inkjet printing, fuel and oil ejection and bio-technology.

Flexural plate waves or Lamb waves have also been proposed for pumping, agitating and enhancing biochemical reactions [Nguyen & White 1999], with the principle that fluid motion via the travelling flexural wave in an AlN membrane can be used for the transport of liquids. The potential applications include a micro total analysis system (μTAS), cell manipulating systems, and drug delivery systems [Meng et al 2000]. However, there are few studies on microfluidic applications based on the AlN acoustic wave devices, which is a potentially very interesting research topic.

7. Future trends for AlN devices for lab-on-a-chip

The elements required for operating detection as part of a lab-on-a-chip system include: (1) transportation of liquids such as blood or biofluids containing DNA/proteins into an area on which probe molecules have been pre-deposited, (2) mixing/reaction of the extracted DNA or proteins with oligonucleotide or the antibody binders, and (3) detection of an associated change in the physical, chemical, mechanical or electrical signals. Thin film based acoustic wave devices can be used to fabricate lab-on-chip bio-detection systems, which combine the functions of microdroplet transportation, mixing and bio-detection.

Device integration at the device, wafer and system level is critical issue for the lab-on-chip fabrication. Wafer level integration of AlN FBAR device with CMOS fabrication has been reported by Campanella et al 2008. It has electrical connection between FBAR and CMOS. Sharma et al 2010 have fabricated a shear mode AlN solidly mounted resonator microfluidic sensor, which is fully IC compatible, integrating a SMR sensor chip with a PDMS microfluidic channel system. The c-axis AlN film has been used to generate shear mode wave and the AlN SMR device operated at the 1.2 GHz range, with a Q factor of 100 in water.

Acoustic wave technologies can be integrated with other technologies, such as the surface plasma resonance (SPR) method [Homola et al 1999]. SPR sensor technology has been commercialized and SPR biosensors have become an important tool for characterizing and qualifying biomolecular interactions. A combination of SAW microfluidics and SPR sensing would appear to be sensible for both microfluidic and detection functions. A potential problem is that the surface temperature change induced by acoustic excitation may cause changes in refractive index, which is used for SPR sensor detection. A pulse mode SAW signals can be used to minimize this effect. Acoustic wave microfluidic devices can also be combined with liquid or gas chromatography, which can be used to identify the protein or molecules by mass spectroscopy [Sokolowski et al 2006]. Integration of a SAW with optical methods enables the simultaneous qualification of biological soft layers formed on the sensor surface under different density, viscosity, thickness and water content.

For digital microfluidics, there is a need to precisely and continuously generate liquid droplets. AlN acoustic wave technology can be used for the ejection of liquid droplets, but it is rather difficult to precisely control the micro-droplet generation. A potential technology to overcome the drawbacks is to combine electrowetting-on-dielectrics (EWOD) [Li et al 2009] with SAW-microfluidics. In the past ten years, EWOD technology has been successfully developed to dispense and transport nanolitre to microlitre bio-samples in droplet form at the exact volume required [Fair 2007]. However, one of the weaknesses is that EWOD technology does not provide efficient micro-mixing, and requires the integration of other technologies e.g. CMOS to realise bio-reaction and biosensing. A novel idea is to integrate the thin films based SAW devices with the EWOD device to form lab-on-a-chip equipped

with well developed functionalities of droplet generation, transportation by EWOD, mixing and biosensing using SAW technology [Li et al 2010].

Acoustic wave devices can easily be integrated with standard CMOS technology. Dual SAW or FBAR devices can be fabricated next to each other, so that the neighbouring devices can be used as a sensor-reference combination. One of the devices without pre-deposited probe molecules can be used as a reference, while the other one with probe molecules can be used to sense. Using such a combination, the errors due to temperature drift or other interference on the sensing measurement can be minimized. Multi-sensor arrays can easily be prepared on a chip and a judicious selection of different immobilized bio-binders enables the simultaneous detection of multiple DNA or proteins, leading to accurate diagnosis of a disease or detection of multiple diseases in parallel. The creation of these cost-effective sensor arrays can increase the functionality in real time and provide parallel reading functions.

Currently, one limitation of acoustic wave device applications is that they require expensive electronic detection systems, such as network analyzers. A final product aimed at the end user market must be small, portable and packaged into a highly integrated cost effective system. The detection of a resonant frequency can be easily realized using standard oscillator circuits which can measure the sensor losses based on a portable device. The required purposely built electronics for acoustic wave sensing are being developed, but at present they are still bulky and heavy. Fabrication of portable thin film based acoustic wave detection devices is also promising and will enable the system size to be minimised along with reducing the power consumption. A wireless RF signals can be used to remotely power and control/monitor physical, chemical and biological quantities by using acoustic wave devices, without requiring a directly wired power supply. Currently for a lab-on-chip device, sample pre-treatment, purification and concentration, as well as a good interface between the user and the integrated sensing system also need to be developed. A simple, robust, cheap packaging method is also critical for commercialization.

8. Summary

AlN films have good piezoelectric properties and a high electro-mechanical coupling coefficient, and are hence a promising technology for the fabrication of fully automated and digitized microsystems with low cost, fast response, reduced reagent requirement and precision. In this chapter, recent development on preparation and application of AlN films for acoustic wave-based microfluidics and bio-sensors has been discussed. The microstructure, texture and piezoelectric properties of the films are affected by sputtering conditions such as plasma power, gas pressure, substrate material and temperature as well as film thickness. AlN acoustic wave devices can be successfully used as bio-sensors, based on a biomolecular recognition system. Among these biosensors, surface acoustic wave, Lamb wave and film bulk acoustic resonator devices using inclined films are promising for applications in highly sensitive bio-detection systems for both dry and liquid environments. The acoustic wave generated on the AlN acoustic devices can also induce significant acoustic streaming, which can be employed for mixing, pumping, ejection and atomization of the fluid on the small scale depending on the wave mode, amplitude and surface condition. An integrated lab-on-a-chip diagnostic system based on these thin film based acoustic wave technologies has great potential, and other functions such as droplet creation, cell sorting, as well as precise bi-detection can be obtained by integration with other advanced technologies.

9. Acknowledgement

10. References

Akiyama, M. T., Kamohara, K. Kano, et al, 2008, Appl. Phys. Lett. 93: 021903.

Akiyama, M., K. Nagao, N. Ueno, et al., 2004. Vacuum, 74: 699-703.

Akiyama, M., N. Ueno, H. Tateyama, et al. 2005. J. Mater. Sci., 40: 1159-1162.

Assouar M. B., O. Elmazria, L. Brizoual, et al, 2002. Diam. Relat. Mater. 11: 413-417.

Aubert T., O. Elmazria, B. Assouar, et al, Appl. Phys. Lett., 96 (2010) 203503.

Auger M. A., L. Vazquez, O. Sanchez, et al, 2005. J. Appl. Phys., 97: 123528.

Baek, J., J. Ma, M.F. Becker, J.W. Keto and D. Kovar, Thin Solid Films 515 (2007), p. 7096.

Ballantine, D. S., R. M. White, S. J. Martin, A. J. Ricco, E. T. Zellers, G. C. Frye, H. Wohltjen, 1996, Acoustic Wave Sensors, Theory, Design and Physical-Chemical Applications, Academic Press.

Barie, N. and M. Rapp; 2001. Biosensors & Bioelectron. 16: 978.

Benda V., M. Cernik and D. Stepkova, Microelectron. J. 29 (1998), p. 695.

Benedic, F., M. B. Assouar, P. Kirsch, P, et al. 2008. Diam. Relat. Mater., 17: 804-808.

Benetti, A., D. Cannata, F. Di Pietrantonio, et al. 2006. Thin Sold. Films, 497: 304-308.

a-Benetti, A., D. Cannata, F. Di Pietrantonio, et al. 2005. IEEE Trans. Ultra. Ferro. Freq. Control. 52, 1806-1811.

b-Benetti M., APL. 87 (2005) 173504

Bjurstrom, J., D. Rosen, I. Katardjiev, V. M. Yanchev and I. Petrov; 2004. IEEE Trans. Ultrason. Ferroelectric and Freq. Control; 51: 1347-1353.

Brizoual, Le L., O. Elmazria O, F. Sarry, M. El Hakiki, A. Talbi, P. Alnot, 2006. Ultrasonics. 45: 100-103.

Brizoual, Le, L. and Elmazria, O, 2007. Diamond. Realt. Mater., 16: 987-990.

Buttry, D. A. and M. D. Ward, 1992. Chem. Rev. 92: 1355.

Caliendo, C., P. Imperatori, E. Cianci, 2003. Thin Solid. Films, 441: 32-37.

Caliendo C., P. Imperatori, Appl. Phys. Lett. 83 (2003) 1641

Campanella et al 2008. IEEE Device Lett., 29 (2008) 28-30.

Kar J P, Bose G, Tuli S, Dangwal A, Mukherjee S, J. Mater. Engng Perf. 18 (2009) 1046-1051.

Chen, Q. M. and Q. M. Wang. 2005. Appl. Phys. Lett. 86: 022904.

Cheng, C. C. Chen, Y.C. Horng R. C. et al. 1998. J. Vac. Sci. Technol., 16: 3335-3340.

Cherng, J. S., C. M. Lin, T.Y. Chen, 2008. Surf. Coat. Technol., 202: 5684-5687.

Cherng, J. S. and D.S. Chang, 2008. Thin Solid Films, 516: 5293-5295.

Cherng, J. S., T.Y.Chen, C. M. Lin, 2009. Ferroelectric, 380: 89-96.

Cheung, T. T. and C. W. Ong, 2004. Diamond Relat Mater., 13: 1603-1608.

Chiu, C S, H. M. Lee, C. T. Kuo, et al. 2008. Appl. Phys. Lett. 93: 163106.

Chiu, C S. 2008. Appl. Phys. Lett., 93: 163106.

Chiu, K H, J. H. Chen, H. R. Chen et al, 2007. Thin Solid Films, 515: 4819-4825.

Chono, K, N. Shimizu, Y. Matsu, J. Kondoh, S. Shiokawa. 2004. Jap. J. Appl. Phys. 43: 2987.

Chou, CH; Lin, YC; Huang, JH, et al. 2006. Integrat. Ferro., 80: 407-413.

Chung, G S, and K.S. Kim 2007, Electron. Lett. 43 (2007), p. 832

Clement, M., L. Vergara, J. Sangrador, et al, 2004. Ultrasonics, 42 : 403-407.

Clement, M., E. Iborra, J. Sangrador, et al. 2003. J. Appl. Phys., 94: 1495-1500.

Clement, M., J. Olivares, E. Iborra, et al., 2009. Thin Solid Films. 517: 4673-4678.

Corso, C. D., A. Dickherber, , W. D. Hunt. 2007. J. Appl. Phys. 101: 054514.

Cote, G. L., R. M. Lec, M. V. Pishko, 2003. IEEE Sens. J., 3: 251-266.

Dickherber, A., C. D. Corso, W. D. Hunt, 2008. Sens Actuat., A 144: 7-12.

Duhamel, R., L. Robert, H. Jia, et al, 2006. Ultrasonics, 44: e893-e897.

Elmazria, O., V. Mortet, M. El Hakiki, et al. 2003. IEEE Trans. Ultrasonic. Ferro. Freq. Cont. 50 : 710-715.

Elmazria, O., Sergei Zhgoon, Laurent Le Brizoual, Frédéric Sarry, Dmitry Tsimbal, and Mohammed Abdou Djouadi, Appl. Phys. Lett., 95, 233503 _2009.

Engelmark, F., G. F. Iriarte and I. V. Katardjiev. 2002. J. Vac Sci Technol B. 20 : 843-848.

Engelmark, F., G. Fucntes, I. V. Katardjiev, et al . 2000. J. Vac Sci Technol A. 18: 1609-1612.

Fair, R. B. 2007. Microfluid Nanofluid, 3: 245-281

Fardeheb-Mammeri, M., B. Assouar, O. Elazria, et al, 2008. Diam. Relat. Mater., 17: 1770-1774.

Franke, T. A. and A. Wixforth, 2008. Chem Phys Chem, 9: 2140-2156.

Fu, Y. Q., J.K. Luo, X. Du, A.J. Flewitt, Y. Li, A. Walton, W.I. Milne, 2010. Sens. Actuat. B. 143: 606-619.

Fu, Y. Q., X.Y.Du, J.K.Luo, A.J.Flewitt, M.I.Milne, 2008. IEEE Sens., 1-3: 478-83.

Galipeau, D.W., P. R. Sory, K. A. Vetelino, R. D. Mileham, 1997, Smart. Mater. Struct. 6: 658.

Gao XD, E.Y. Jiang, H.H. Liu, G.K. Li, W.B. Mi, Z.Q. Li, P. Wu and H.L. Bai, Phys. Status Solidi (a) 204 (4) (2007), p. 1130.

Gizeli, E. 1997. Smart. Mater. Struct. 6: 700.

Grate, W. J., S. J. Martin, R. M. White, 1993. Anal Chem., 65: 940.

Grate JW, 2000, Chem. Rev, , 100 (7), pp 2627–2648

Hakiki M. E., O. Elmazria, P. Alnot, 2007. IEEE transactions on Ultrasonics, Ferro. Freq. Control, 54: 676-681.

Hara, M., J. Kuypers, T. Abe, et al. 2005. Sens. Actuat., A 117: 211-216.

Hirata S., K. Okamoto, S. Inoue, et al. 2007. J. Solid State Chem. 180: 2335-2339.

Si-Hong Hoang and Gwiy-Sang Chung, Microelectronic Engineering, Volume 86, Issue 11, November 2009, Pages 2149-2152.

Homola, J., S. S. Yee, G. Gauglitz, 1999. Sens. Actuat., B 54: 3-15.

Hong, H. S. and Chung, G. S. 2009. J. Korean Phys. Soc. 54: 1519-1525.

Hoummady, M., A. Campitelli, W. Wlodarski, 1997, Smart. Mater. Struct. 6: 647.

Huang, C. L., K. W. Tay, L. Wu. 2005. Solid State Electro. 49: 219-225.

Huang, C. L.; K. W. Tay, L. Wu. 2005. Jap. J. Appl. Phys., 44: 1397-1402.

Iborra, E., M. Clement, J. Sangrador, et al, 2004. IEEE Trans. Ultras. Ferroelectr. Freq. Control, 51: 352-358.

Imura M et al, 2010], Kiyomi Nakajima, Meiyong Liao, Yasuo Koide, Hiroshi Amano, Journal of Crystal Growth 312 (2010) 368–372.

Iriarte, G F,, F. Engelmark and I.V. Katardjiev, J. Mater. Res. 17 (2002), p. 1469.

Iriarte, G.F. 2003. J. Appl. Phys., 93: 9604-9609.

Ishihara, M, K. Yamamoto, F. Kokai, et al. 2000. Vacuum, 59: 649-656.

Jacoby, B. and M. Vellekoop, 1997. Smart. Mater. Structu., 6: 668-679.

Jagadish, C. and S. J. Pearton, 2006. Zinc oxide bulk, thin films and naoctstructures: processing, properties and applications, Elseveier.

Jasinki J, Z. Liliental-Weber, Q. S. Paduano, D. W. Weyburne, 2003. Appl. Phys. Lett., 83: 2811.

Ji, X. H., S. P. Lau, G. Q. Yu, et al, 2004. J. Phys. D. 37: 1472-1477.

Josse, F., F. Bender, R. W. Cernosek. 2001. Anal. Chem. 73: 5937.

Kang, Y. R., S. C. Kang, K. K. Park, Y. K. Kim, S.W. Kim and B. K. Ju. 2005. Sens. Actua. A117: 62.

Kao, K. S., C.C. Cheng, Y.C. Chen, Y. H. Lee, 2003. Appl. Phys., A76: 1125-1127.

Kar J P, Bose G, Tuli S, Dangwal A, Mukherjee S, J. Mater. Engng Perf. 18 (2009) 1046-1051.

Kern, R. S., L. B. Rowland, S. Tanaka, et al. 1998. J. Mat. Res. 13: 1816-1822.

Khan, F. A. et al. 2006. Mater. Sci. Engng, B 95: 51-4.

Kim, E. K., T. Y. Lee, H. S. Hwang, et al.; 2006. Superlatt. & Microstr. 39: 138.

Kim, S. H., J. H. Kim, D. D. Park, G. Yoon, 2001. J. Vac. Sci. Technol., B 19: 1164-1168.

Kirsch, P., M. B. Assouar, O. Elmazria, et al. 2006. Appl. Phys. Lett., 88: 223504.

Kovacs, G., G.W. Lubic, M. J. Vellekoop, A. Venema, 1992. Sens. Actuat., A 43: 38-43.

Kovacs. G. and M. Venema. 1992. Appl Phys Lett. 61: 639.

Kumagai Y., T. Yamane and A. Koukitu, J. Crystal Growth 281 (2005), p. 62.

Kumar, K. S. A. and S. M. Chen, 2008. Analytical Letters 41: 141–58.

Kuznestsova, L. A. and W.T. Coakley, 2007. Biosensors and Bioelectronics 22: 1567-1577.

Lange, K., B. E. Rapp, M. Rapp, 2008. Anal. Bioanal. Chem. 391: 1509-1519.

Lanz R. and P. Muralt, IEEE Trans. Ultrason. Ferr. Freq. Control 52 (6) (2005), p. 936.

Lee, C. K., S. Cochran, A. Abrar, K. J. Kirk, F. Placido, 2004. Ultrasonics, 42: 485-490.

Lee, H.C., J. Y. Park, K. H. Lee, et al. 2004. J. Vac. Sci. Technol. B, 22: 1127-1133.

Lee, J. B., M. H. Lee, C. K. Park, et al. 2004. Thin Solid Films, 447: 296-301.

Lee S. H., K.H. yoon, J. K Lee, 2002. J Appl. Phys., 92: 4062-4069.

Lee, S. H, J. K. Lee, K. H. Yoon. 2003. J. Vac. Sci. Technol., A, 21: 1-5.

Lee T Y, Song J T, Thin Solid Films, 2010, In press.

Li, Y., B.W. Flynn, W. Parkes, et al., Conference of ISSDERC 2009, in press.

Lim, W. T., B. K. Son, D. H. Kang, C. H. Lee, 2001. Thin Solid Film, 382: 56-60.

Lin, Z. X., S. Wu, R. Y. Ro, et al. 2009. IEEE. Trans. Ultraonics. Ferroelec. Freq. Control, 56: 1246-1251.

Ling C M, T T Yen, Y, J. Lai, et al IEEE Trans Ultras. Ferro, Freq. Control, 57 (2010) 524-532.

Lindner, G., 2008. J. Phys. D. 41: 123002.

Liu, Z. F., F.K. Shan, Y.X. Li, B.C. Shin and Y.S. Yu, 2003. J. Crystal Growth 259: 130.

Liu, J. M., N. Chong, H. L. W. Chan, et al. 2003. Appl. Phys., A, 76: 93-96.

Lu Y F, Ren Z M, Chong, TC Cheng, BA, Chow SK, wang J P., J Appl. Phys. 87 (2000) 1540.

Lucklum, R. and P. Hauptmann. 2003. Meas. Sci. Technol. 14: 1854.

Luginbuhl, P., S. D. Collins, G. A. Racine, M. A. Gretillat, N. F. De Rooij, K. G. Brooks, N. Setter. 1997. J. MEMS, 6: 337-346.

Luo, J. K., Y.Q. Fu, Y. F. Li, X.Y. Du, A.J. Flewitt, A. Walton, W. I. Milne, 2009. J. Micromech. Microeng., 19: 054001.

Marx, K. A., 2003. Biomacromolecules. 4: 1099.

Mchale, G. 2003. Meas. Sci. Technol. 14: 1847.

Meng, A. H., N.T. Nguyen and R.M. White, 2000. Biomed. Microdev. 2: 169–174

Mortet, V., M. Nesladek, K. Haenen, et al. 2004. Dia. Relat. Mater., 13: 1120-1124.

Muralt P, 2008. J. Am. Ceramic. Soc., 91: 1385-1396.

Muralt, P., N. Ledermann, J. Baborowski, et al. 2005. IEEE Trans. Ultrasonics, Ferroelectr. Frequen. Control. 52: 2276.

Murochim, N., M. Sugimoto, Y. Matui, J. Kondoh, 2007. Jap. J. Appl. Phys., 46: 4754.

Naik, R. S., R. Reif, J.J. Lutsky and C.G. Sodini, 1999. J. Electrochem. Soc. 146: 691.

Newton, M. I., M. K. Banerjee, T. K. H. Starke, S. M. Bowan, G. McHale, 1999. Sensor & Actuat. 76: 89.

Nguyen, N. T. and R. T.White. 1999. Sens. & Actuat. 77: 229-36.

Okamoto, K., S. Inoue, T. Nakano, et al. 2008. Thin Solid Films, 516: 4809-4812.

Okamoto M., M. Yamaoka, Y.K. Yap, M. Yoshimura, Y. Mori and T. Sasaki, Diamond Relat Mater 9 (2000), p. 516.

O'Hanlon JF, A User's Guide to Vacuum Technology (2nd. ed.), John Wiley and Sons, Hoboken, NJ (1989).

Paci, B., A. Generosi, V. R. Albertini, et al. 2007. Sens. Actuat., A 137: 279-286.

Pandey D.K., R.R. Yadav, Temperature dependent ultrasonic properties of aluminium nitride, Applied Acoustics 70 (2009) 412–415.

Pandey DK, Yadav RR, Appl. Acoustics, 70 (2009) 412-415.

Pearton, S. J., D. P. Norton, K. Ip, Y. W. Heo, T. Steiner, 2005. Prog. Mater. Sci. 50: 293.

Renaudin, A., P. Tabourier, V. Zhang, J.C. Camart, C. Druon. 2006. Sensor & Actuat. B113: 387.

Rey-Mermet, S., J.Bjurstrom, D.Rosen and I.Petrov. 2004. IEEE Trans. Ultrason. Ferroelectric and Freq. Control; 51: 1347.

Ruby, R. 2007. IEEE Ultrasonics Symp. Proc. 1-6 : 1029-1040.

Sanchez, G., A. Wu, P. Tristant, et al. 2008. Thin Solid. Films, 516: 4868-4875.

Sano, A., Y. Matsui, S. Shiokawa, 1998. Jap. J. Appl. Phys. 37: 2979.

Saravanan, S., E. Berenschot, G. Krijnen, M. Elwenspoek, 2006. Sens. Actuat., A130-131: 340-345.

Sharma G., L. Liljeholm, J. Enlund, J. Bjurstorm, I. Katardjiev, K. Hjort, Sens. Actuat., A 159 (2010) 111-116.

Sheng, T. Y., Z.Q. Yu, GJ Collins, 1988. Appl. Phys. Lett., 52: 576.

Shih, W. C., R. C. Huang, Y. K., Peng, et al. 2009. Ferroelectr., 380: 20-29.

Shiokawa, S., J. Kondoh, 2004. Jap. J. Appl. Phys., 43: 2799-2802.

Shiokawa, S., Y. Matsui and T. Morizum. 1989. Jpn. J. Appl. Phys. 28: 126.

Sritharan, K., C. J. Strobl, M. F. Schneider, A. Wixforth, 2006. Appl. Phys. Lett., 88: 054102.

Strobl, C. J., Z. Guttenberg, A. Wixforth; 2004. IEEE Trans. Ultrasonics, Ferrelectric and freq. Control. 51: 1432.

Sudhir G.S., H. Fujii, W.S. Wong, C. Kisielowski, N. Newman and C. Dieker et al., Appl Surf Sci 127–129 (1998), p. 471.

Takagaki, Y., P.V. Santos, E. Wiebicke, et al, 2002. Appl. Phys. Lett. 81: 2538-2540.

Tan, S. S., M. Ye, A. G. Milnes, 1995. Solid State Electro., 38: 17.

Tanosch, K., et al, Sens. Actuato, 2006. A132: 658-663.

Teles F R R, L. P. Fonseca, 2008. Talanta, 77: 606-623.

Toegl, A., J. Scribe, A. Wixforth, C. Strobl, C. Gauer, Z.V. Guttenburg. 2004. Anal. Bioanal. Chem. 379: 69.

Toegl, A., R. Kirchner, C. Gauer, A. Wixforth, 2003. J. Biomed. Technol., 14: 197.

Tseng, W. K., J. L. Lin, W. C. Sung, S. H. Chen, G. B. Lee; 2006. J. Micromech. Microeng. 16: 539.

Vashaei Z., T. Aikawa, M. Ohtsuka, H. Kobatake, H. Fukuyama, S. Ikeda and K. Takada, Journal of Crystal Growth, 311, 2009, 459-462.

Vellekoop, M. J., 1998. Ultasonics. 36: 7.

Vergara, L., M. Clement, E. Iborra, et al. 2004. Diam. Relat. Mater., 13: 839-842.

Weber, J., W. M. Albers, J. Tuppurainen, M. Link, R. Gabl, W. Wersing, M. Schreiter, 2006. Sensors & Actuat. A128: 84-88.

H. Windischmann, Crit. Rev. Solid State Mater. Sci. 17 (1992), p. 547.

Wingquist, G., J. Bjurstrom, L. Liljeholm, et al, 2007. Sens. Actuat., B123: 466-473.

Wingquist, G., J. Bjurstrom, A.C. Hellgren, I. Katardjiev, 2007. Sens. Actuat., B127: 248-252.

Wingqvist G. V. Yantchev, Katardjiev, Sens. Actuat. A., 148 (2008) 88-95.

a-Wingqvist G., Anderson, H., Lennartsson, Weissbach T, Yantchev V., Lyoyd A, Spet Z., Bios. Bioelectron., 24 (2009) 3387-3390.

b-Wingqvist G, L Arapan, V Yantchev and I Katardjiev, J. Micromech. Microeng. 19 (2009) 035018. Wixforth, A., C. Strobl, C. Gauer, A. Toegl, J. Sciba, Z. V. Guttenberg, 2004. Anal. Biomed. Chem., 379: 982.

Wixforth. A. 2004. Superlattices & Microstruct. 33: 389.

Wohltjen, H., et al. 1997. Acoustic Wave Sensor—Theory, Design, and Physico-Chemical Applications, Academic Press, San Diego:39.

Wu, L., S. Wu, H. T. Song, 2001. J. Vac. Sci. Technol., A19: 167.

Wu, S., R. Ro, Z. X. Lin, M S. Lee. 2008. J. Appl. Phys. 104: 064919.

Wu, S., Y.C. Chen, Y.S. Chang. 2002. Jap. J. Appl. Phys., 41: 4605-4608.

Wu, H. P., L. Z. Wu, S. Y. Du, 2008. J. Appl. Phys., 103: 083546.

Wu, S., R. Y. Ro, Z. X. Lin, et al. 2009. Appl. Phys. Lett., 94: 092903.

Xu J. Thakur J S., Zhong F., Ying H., Auner G W, J Appl. Phys. 96 (2004), 212-217.

Xu, J., J. S. Thakur, G. Hu, et al. 2006. Appl. Phys. A, 83: 411-415.

Yanagitani, T. and M. Kiuchi; 2007. J. Appl. Phys. 102: 044115.
Yantchev and Katardjiev 2007 IEEE Trans. Ultrason. Ferroelectr. Freq. Control 54 87–95
Yang, P. F., S. R. Jian, S. Wu, et al. 2009. Appl. Surf. Sci., 255: 5984-5988.
Zhang, D., J. H. Edgar, 2005. Mater Sci. Engng R, 48: 1-46.
Zhang H, Kim E S, 2005, J MEMS, 14, 699-706.
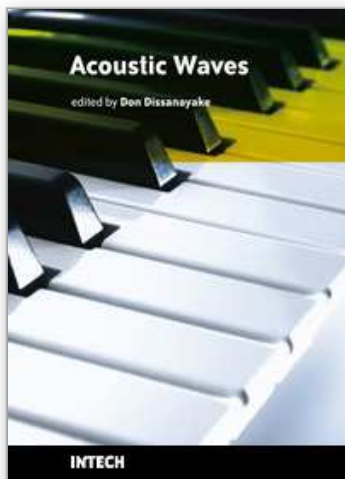
Acoustic Waves

Edited by Don Dissanayake

SAW devices are widely used in multitude of device concepts mainly in MEMS and communication electronics. As such, SAW based micro sensors, actuators and communication electronic devices are well known applications of SAW technology. For example, SAW based passive micro sensors are capable of measuring physical properties such as temperature, pressure, variation in chemical properties, and SAW based communication devices perform a range of signal processing functions, such as delay lines, filters, resonators, pulse compressors, and convolvers. In recent decades, SAW based low-powered actuators and microfluidic devices have significantly added a new dimension to SAW technology. This book consists of 20 exciting chapters composed by researchers and engineers active in the field of SAW technology, biomedical and other related engineering disciplines. The topics range from basic SAW theory, materials and phenomena to advanced applications such as sensors actuators, and communication systems. As such, in addition to theoretical analysis and numerical modelling such as Finite Element Modelling (FEM) and Finite Difference Methods (FDM) of SAW devices, SAW based actuators and micro motors, and SAW based micro sensors are some of the exciting applications presented in this book. This collection of up-to-date information and research outcomes on SAW technology will be of great interest, not only to all those working in SAW based technology, but also to many more who stand to benefit from an insight into the rich opportunities that this technology has to offer, especially to develop advanced, low-powered biomedical implants and passive communication devices.

How to reference

In order to correctly reference this scholarly work, feel free to copy and paste the following:

Stuart Brodie and Richard Fu (2010). Thin Film Based Acoustic Wave Devices for Microfludicis and Bisensing Applications, Acoustic Waves, Don Dissanayake (Ed.), ISBN: 978-953-307-111-4, InTech, Available from: http://www.intechopen.com/books/acoustic-waves/thin-film-based-acoustic-wave-devices-for-microfludicis-and-bisensing-applications

INTECH
open science | open minds